Mukaddas *et al.*
Journal of Materials Science: Composites (2025) 6:12
https://doi.org/10.1186/s42252-025-00075-9

Functional Composite Materials

RESEARCH Open Access

Physio-chemical analysis and characteristics of nanoclay hybrid polyamide biocomposite

Ahmad Musa Mukaddas[1,2], Farah Nora Aznieta Abdul Aziz[4], Khalina Abdan[2,3*] and S. Ayu Rafiqah[2]

Abstract

The quest for sustainable and high-performance fibre reinforced polymer composite materials enhanced with compatibilisers has garnered significant attention for structural applications such as railway sleepers. This study explores the effects of nanoclay incorporation on the physio-chemical, mechanical, thermal, and morphological properties of hybrid polyamide biocomposites reinforced with treated kenaf and glass fibres. Aimed at addressing the limitations of natural fibre composites in terms of dimensional stability and moisture resistance, and mechanical robustness. hybrid composites were fabricated using varying contents of nanoclay (0–5 wt%) and fibre compositions (20–50 wt.%). Standardized tests including ASTM-based mechanical evaluations, thermogravimetric analysis (TGA), Fourier-transform infrared spectroscopy (FTIR), and scanning electron microscopy (SEM) were employed. The optimal formulation (E3-2) containing 30% hybrid fibre and 3% nanoclay exhibited superior performance, achieving a flexural strength of 85.9 MPa, impact toughness of 35.30 kJ/m^2, tensile modulus of 6.9 GPa, and water absorption of just 3.42%, thereby surpassing ISO 12856–1 and FFU standards. Nanoclay at 3 wt% was found to significantly enhance thermal stability and interfacial bonding while minimising moisture uptake. However, higher nanoclay concentrations led to particle agglomeration and compromised mechanical integrity. Well dispersed fibres and effective stress transfer mechanisms revealed by SEM analysis, validating the synergy between nanoclay and hybrid fibres. The study concludes that moderate nanoclay loading, especially at 3wt.%, exhibited an optimal balance between performance and processing, making such composites viable for structural applications. It is recommended that future research further optimise fibre treatments and explore long-term durability for broader engineering deployment.

Keywords Nanoclay, Polyamide biocomposite, Hybrid fibres, Flexural strength, Thermal stability, Railway sleeper

Introduction

Nanoclay hybrid polyamide biocomposites represent a significant advancement in materials science, addressing environmental concerns and economic drivers associated with sustainable material development. The incorporation of nanoclay into polyamide matrices enhances mechanical and thermal properties while aligning with contemporary sustainability goals. A compelling economic driver for these composites is the optimization of resource use; improving mechanical properties through nanoclay allows for less material without compromising performance. The addition of nanoclay can significantly enhance tensile strength and stiffness, proving beneficial in reducing material costs while achieving desired mechanical properties [1, 2]. This corresponds with

*Correspondence:
Khalina Abdan
khalina@upm.edu.my
[1] Laboratory of Biocomposite Technology, Institute of Tropical Forestry and Forest Products (INTROP), Universiti Putra Malaysia, 43400 UPM Serdang, Selangor, Malaysia
[2] Department of Civil Engineering Technology, School of Engineering Technology, Federal Polytechnic, BauchiBauchi State 0231, 740005, P.M.B., Nigeria
[3] Department of Agriculture and Biotechnological Engineering, Faculty of Engineering, Universiti Putra Malaysia, 43400 UPM Serdang, Selangor, Malaysia
[4] Housing Research Centre (HRC), Department of Civil Engineering, Faculty of Engineering, Universiti Putra Malaysia, 43400 UPM Serdang, Selangor, Malaysia

findings highlighting the economic advantages of utilizing low-cost natural materials, such as montmorillonite, due to their high aspect ratio and reinforcing capabilities [3]. Recent research further highlights that maintaining nanoclay concentrations between 3–5 wt.% is critical to avoiding agglomeration and ensuring optimal dispersion, which is essential for maximizing mechanical reinforcement (Mylsamy et al., [4]).

The hybridization of natural and synthetic fibres in polyamide matrices represents a significant advancement in composite material science. By blending the advantages of both fibre types, researchers enhance mechanical properties while mitigating inherent weaknesses of natural fibres in engineered applications. Natural fibres such as kenaf, bamboo, and sisal are valued for sustainability and biodegradability but exhibit lower strength and poor moisture resistance compared to synthetic fibres like glass and carbon. For instance, bamboo fibre-reinforced polyamide composites demonstrate effective hydrogen bonding, leading to improved mechanical compatibility without extensive fibre treatment [5]. This illustrates the potential of natural fibres to bond effectively with polar matrices, critical for overall hybrid composite performance. Further research highlights the importance of hybridization in balancing cost and mechanical performance. Synthetic fibres, while stronger, face challenges regarding recyclability and environmental impact. The hybrid approach leverages mechanical advantages from synthetic materials while addressing economic factors and making it compelling for industries such as automotive and aerospace [6, 7]. Moreover, studies suggest that bamboo-glass-nanoclay hybrids exhibit superior dimensional stability and moisture resistance, which broadens their potential in high-humidity applications (Mylsamy et al., [4]).

The challenge of enhancing dimensional stability of polyamide composites has garnered considerable research interest, particularly through the synergistic effects of fibre hybridization and nanoclay incorporation. Various studies have elucidated how these methodologies improve mechanical and thermal properties of polyamide-based materials, ultimately addressing dimensional instability. Fibre hybridization significantly enhances the mechanical properties of composites. In 2017, [8] highlighted that incorporating hybrid nanoparticles including nanoclay into carbon fibre-reinforced plastics can significantly enhance impact performance, leading to improved durability and structural integrity. This observation aligns with findings by Islam et al. [9], who demonstrated that combining different natural fibres with montmorillonite nanoclay resulted in marked transformation in structure and surface morphology of composite materials. These improvements proved critical in advancing the composite's strength and moisture resistance, essential factors for dimensional stability. Additionally, nanoclay in hybrid fibre composites enhances interfacial adhesion and prevents void formation [10] discussed how the synergistic effects of bamboo and glass fibres combined with nanoclay contribute to improved mechanical and water uptake properties, further validating the role of nanoclay in enhancing composite performance. Such synergy is attributed not only to the physical reinforcement of nanoclay but also to improved interfacial compatibility achieved via the use of maleated compatibilizers such as MAPP, which enhance covalent bonding and reduce microvoid formation (Karthik et al., [11]).

In addition to fibre hybridisation and nanoclay incorporation, the use of compatibilisers has also emerged as a crucial strategy for enhancing interfacial adhesion and reducing void formation in polymer composites. In the study by Zhang et al. [12], polypropylene grafted maleic anhydride (PP-g-MAH) was selected as a compatibilizer to improve the compatibility and interfacial bonding between the polymer matrix consisting of recycled high-density polyethylene (RHDPE) and polypropylene (PP), and glass fibre (GF). The inclusion of PP-g-MAH facilitates stronger chemical interactions at the matrix–fibre interface, promoting improved dispersion and mechanical reinforcement. They adopted a 3 wt.% concentration based on performance and industrial best practices, which had demonstrated its effectiveness in enhancing composite performance while maintaining a balance between mechanical properties and material cost. Similarly, the use of silane coupling agents and alkaline-treated fibres, as reviewed by Karthik et al. [11], has proven effective in further reducing moisture sensitivity and enhancing tensile and flexural properties in nanoclay-based fibre-reinforced systems.

Natural fibre-reinforced polymer composites have emerged as highly valued materials in response to the growing demand for sustainable and environmentally friendly alternatives across various industries (Krishnasamy et al., [13]). Beyond their intrinsic advantages—such as low cost, renewability, and biodegradability. The performance of natural fibres can be significantly enhanced through surface modifications. Treatments with additives such as silane coupling agents, graphene oxide, or nano-metal particles like nano-silver and nano-titanium dioxide have been shown to improve interfacial adhesion and mechanical properties, making these composites more suitable for specialised applications (Raj et al., [14]). Furthermore, green alternatives to traditional chemical treatments which includes enzymatic, fungal, and plasma-based modifications offer environmentally

benign pathways for improving fibre surface energy and bonding without compromising biodegradability (Karthik et al., [11]).

Significant strides in bio-based products are constrained by the intrinsic hydrophilicity of lignocellulosic plant fibers, whose hydroxyl-rich surfaces bond poorly with hydrophobic polymer matrices. Traditional adhesion-enhancing chemistries—such as mercerization, silanization, acetylation, permanganate or peroxide oxidation, benzoylation, stearic acid and isocyanate treatments are increasingly questioned for their environmental and practical drawbacks. Their study critically evaluates emerging, low-impact alternatives which includes plasma processes and fungal, enzymatic, or bacterial treatments and detailing how they reengineer fiber surfaces and ultimately improve composite performance.

The analysis of void content in natural fibres used with polyamide matrices, particularly in composite materials such as carbon fibre (CF) and various polyamide combinations, is essential for understanding mechanical properties and performance. Microscopic examination techniques, especially electron microscopy and various imaging methods, play a critical role in quantifying and analyzing void structures, their distributions, and impacts on composite properties. Recent studies have highlighted that voids significantly affect mechanical properties of fibre-reinforced composites. For instance, Hu et al. demonstrated that reducing void content can lead to notable increases in flexural strength of polyamide composites, although the study primarily discusses resin matrix behaviors rather than direct correlation with specific void content levels, requiring cautious interpretation of findings [15]. In 2018, [16] indicated that higher void levels contribute to premature failure in laminated composites due to insufficient load transfer, leading to earlier initial filament breakage, supporting the claim regarding detrimental effects of voids in composite materials. Similarly, [17] emphasized the importance of accurately determining void content using advanced microscopy techniques, which can reveal microstructural characteristics critical for optimizing composite performance. Recent microscopy studies confirm that nanoclay additions combined with appropriate compatibilizer strategies effectively reduce voids and enhance impact strength, enabling better load transfer and resistance to environmental stress (Mylsamy et al., [4]).

Recent studies have extensively analyzed various natural fibre types in polyamide-nanoclay composites, highlighting performance characteristics and strength improvements attributable to different fibre reinforcements and nanoclay incorporation. Natural fibres such as jute, banana, coconut, and Napier grass demonstrate unique properties that, when properly combined with nanoclay reinforcements, yield composites with enhanced mechanical performance. The incorporation of nanoclay into hybrid polyamide composites has garnered significant attention due to its potential to enhance mechanical properties and overall performance. Optimal concentration of nanoclay plays a critical role in achieving desired property enhancements. Research indicates that nanoclay can improve barrier properties of polyamide composites up to a certain threshold. It was also demonstrated that PA6/nanoclay composite films exhibited improved oxygen barrier properties, with increases in nanoclay loading resulting in notable mechanical property enhancements by researcher in ref [18]. Specifically, studies highlighted that the concentrations around 5wt% often yield the best improvements, as higher levels tend to introduce agglomeration, negatively affecting material performance [19]. Similarly, optimization trials indicated that maintaining nanoclay concentration between 4wt% and 10 wt% provides a good balance between enhanced mechanical integrity and processing reliability without compromising material homogeneity [20]. Additionally, Kaynak and Polat emphasized maintaining an optimal concentration limit for flame retardancy, suggesting approximately 5 wt% of nanoclay provides significant improvements without substantial detriment to mechanical properties [21].

Although many studies have investigated the hybridization of fibre-reinforced polymer composites, there remains a gap in comprehensive understanding of nanoclay effects on flexural, impact, and physio-chemical properties of hybrid fibre polymer composites. The current research aims to develop and characterize a novel hybrid composite system by investigating nanoclay incorporation effects on physical, mechanical, thermal and chemical properties of treated natural/synthetic fibre-reinforced polymer composites. This study will evaluate interfacial bonding mechanisms and examine fracture morphology to achieve enhanced dimensional stability, moisture resistance, and overall performance for structural applications.

Materials and methods

Materials

For the experiments, Nylon 6 CM-1017 supplied by Innovate Pultrusion Sdn. Bhd Malaysia, with density of 1.13 g/cm^3, and melt flow index (230 °C/2.16 kg) of 19 g/10 min as polymer matrix. Kenaf fibre from Lembaga kenaf dan Tembakau Negara (LKTN), Kelantan, Malaysia. The kenaf was treated according to [NO_PRINTED_FORM] [22], resulting in treated kenaf fibre (TKF). A short unidirectional 6 mm length glass fibre (GF), and a natural montmorillonite clay (682,632-500G, Sigma-Aldrich), surface-modified, containing 15–35 wt. % Octadecyl

amine, and 0.5–5 wt. % aminopropyl triethoxysaline. monodisperse particles in the form of faint beige powder ≤ 20-micron, bulk density of 200–500 kg/m^3.

Method

Preparation of composite material

In this work, adherence to the following steps is essential to prevent the degradation of fibre-matrix interface, including potential swelling or formation of micro cracks within the composite. Prior to sample preparation, Nylon 6 (PA6) and treated kenaf fibre (TKF) were dried in a ventilated oven at (70 ± 5) °C for 24 h. Then PA6, TKF, GF and nanoclay (NC) were weighed and bagged according to the formulations in Table 1. Previous researchers had indicated that 10, 20, 30, 40, 50, and 60% are the most common wood flour portions by weight used in making starch, polylactic acid (PLA) etc. and reinforced composites [23]. Thus, a total of sixteen mixtures were prepared. Four hybrid fibre-reinforced composite series E2, E3, E4 and E5 containing 20, 30, 40 and 50% hybrid fibres, respectively. For each series, one control (no nanoclay) and three nanoclay modified formulations were produced, denoted for as E2-1, E2-2 and E2-3, where the numerals indicate 1, 3 and 5 wt.% nanoclay. These nanoclay loadings were chosen following Tay et al. [24], who examined hybrid glass/kenaf epoxy composites at the same organomodified nanoclay contents identified in the literature as influential on composite performance. Their findings showed that treated kenaf fibres improved flexural strength and modulus, while higher nanoclay contents (3–5 wt.%) reduced these properties due to agglomeration and poor dispersion. Impact testing established 1 wt% nanoclay as optimal, yielding the lowest absorbed energy and superior dispersion, as confirmed by XRD and SEM analyses.

Mixing was done in an internal mixer—Brabender 815,652 which is manufactured by GmbH & Co KG Duisburg, Germany. The machine is equipped with a counter-rotating twin screw, set at a speed of 50 rpm, with the temperature profile in zones 1–3 set to 230 °C. First, the PA6 was fed into the mixing chamber, after its melting at 5 min, nanoclay was added. After mixing for another 5 min, the GF was fed into the system and mixed for 2–3 min, followed by TKF for another 2–3 min. The total mixing time was 15 (± 1) min. The resulting pellets (granules) were then grinded to prepare the granules using a pilot scale grinder. The granules were then dried in a drying oven (Protech, Gov-100, Malaysia) at 100 °C until they were dry enough for hot pressing in a thermosetting hydraulic compression moulding machine—Technopress–40HC-B, manufactured by Technopress Sdn. Bhd., Malaysia. The dried granules were weighed, poured into a mould, and processed using a compression moulding machine. The procedure involved preheating for 10 min, compressing at 18 MPa for 5 min, and cooling for 2 min. This method followed the approach described in our earlier work [NO_PRINTED_FORM] [22] with modification. The boards were then cut into various tests specimen using the small bandsaw (LB1200F, JM21080021 Makita Corporation,Anjo,Aichi, Japan) and plastic pneumatic mould cutter (ST-7016-HA, GOTECH Testing Machines inc., Taiwan). Finally, the specimens were

Table 1 Composition of the studied formulations

Sample Code	Constituents	PA6 (wt%)	Treated Kenaf Fibre (TKF) (wt%)	Glass Fibre (GF) (wt%)	Nanoclay (wt%)
E2	80PA6 5TKF 15GF	80	5	15	0
E2-1	79PA6 5TKF 15GF 1NC	79	5	15	1
E2-2	77PA6 5TKF 15GF 3NC	77	5	15	3
E2-3	75PA6 5TKF 15GF 5NC	75	5	15	5
E3	70PA6 10TKF 20GF	70	10	20	0
E3-1	69PA6 10TKF 20GF 1NC	69	10	20	1
E3-2	67PA6 10TKF 20GF 3NC	67	10	20	3
E3-3	65PA6 10TKF 20GF 5NC	65	10	20	5
E4	60PA6 15TKF 25GF	60	15	25	0
E4-1	59PA6 15TKF 25GF 1NC	59	15	25	1
E4-2	57PA6 15TKF 25GF 3NC	57	15	25	3
E4-3	55PA6 15TKF 25GF 5NC	55	15	25	5
E5	50PA6 20TKF 30GF	50	20	30	0
E5-1	49PA6 20TKF 30GF 1NC	49	20	30	1
E5-2	47PA6 20TKF 30GF 3NC	47	20	30	3
E5-3	45PA6 20TKF 30GF 5NC	45	20	30	5

kept under control condition (50% relative Humidity and 23 °C) for at least 40 h in a sample storage (APX-155EX, AIPO sample storage, Malaysia) prior to testing. The fabrication processes is illustrated in Fig. 1.

Atmospheric conditions during testing were controlled at 22 ± 5 °C and 44 ± 5% RH using an EXTECH 42280 A datalogger, China. All sample preparations were performed at room temperature.

Physical properties characterisations

Water absorption

The water absorption test was conducted according to international standard [NO_PRINTED_FORM] [25]. Five replicates of samples with dimensions of 50 × 50 × 3.2 mm were dried in an oven maintained at 50 ± 2 °C for at least 24 h, placed in a desiccator, and allowed to cool to room temperature before weighing them to the nearest 0.1 mg. The process was repeated until the specimen mass became constant (mass, m_1).

Mechanical properties characterisation

The flexural strength, flexural modulus, tensile strength and impact toughness of hybrid and hybrid polyamide biocomposites containing nanoclay were evaluated according to the American Standard Testing and Materials (ASTM) for plastic materials. A three-point flexural test, which was set up in accordance with ASTM D 790–14 [26], was conducted to assess the flexural strength of the composites at a test speed of 1.36 mm/min, R1 = 5.0 ± 0.2 mm and R2 = 5.0 ± 0.2 mm. Figure 2 shows the flexural test specimens on the test instrument. All mechanical tests were performed by utilizing a universal testing machine (UTM-30, INSTRON, OHIO, USA), and the strength was calculated by averaging the results obtained from five replicates.

The tensile strength was determined (using the same UTM-30, INSTRON, USA) by performing a tensile test according to the standards stipulated in ASTM D638-14 [27] with specimen preparation following ASTM D638-14 [27] Type IV method, using a gauge length of 115 mm. The size of the tensile test specimen specified in its standard and the clamping method on the test instrument are presented in Fig. 3 and Table 2. Moreover, the test was conducted at a speed of 5 mm/min. The impact absorption test was conducted (using the Izod impact CEAST 9050 series, INSTRON, USA) following the

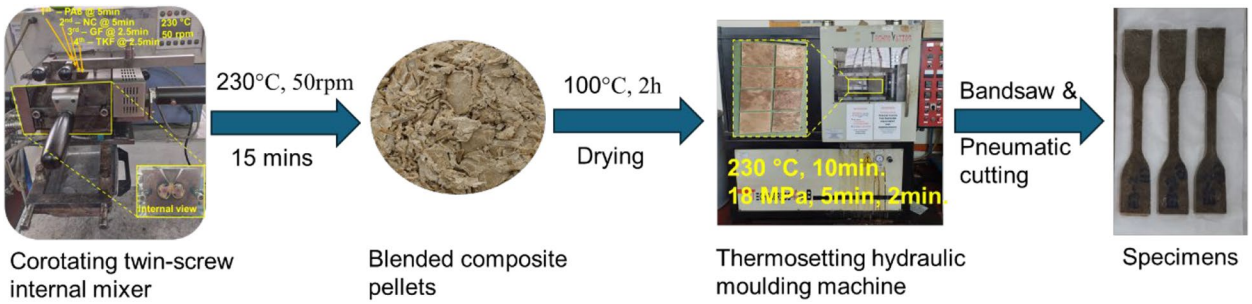

Fig. 1 Composite preparation process

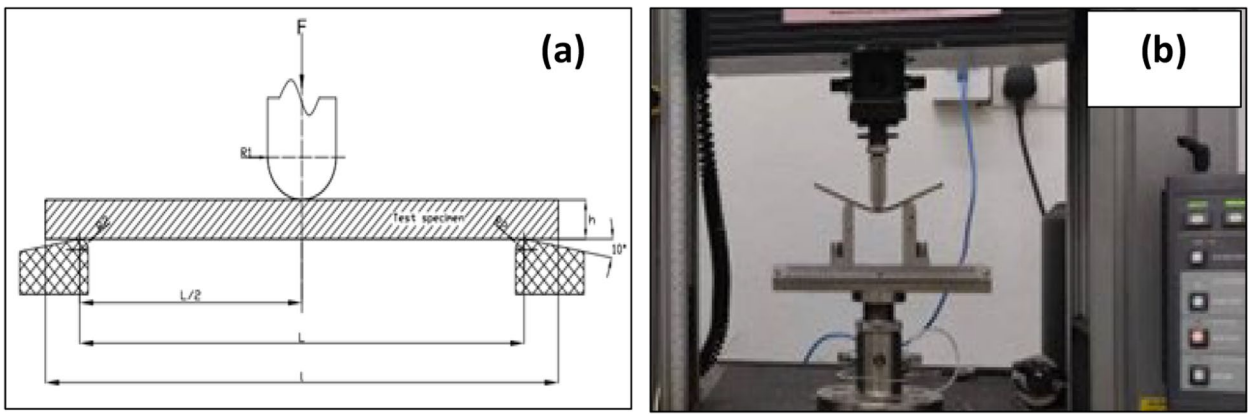

Fig. 2 Flexural test specimen (**a**) specimen diagram in the ASTM standard, (**b**) Specimen on flexural test equipment. (1, test specimen; F, applied force; R1, radius of the loading edge; R2, radius of supports; h, thickness of the specimen; l, length of the specimen; L, length of the span between supports)

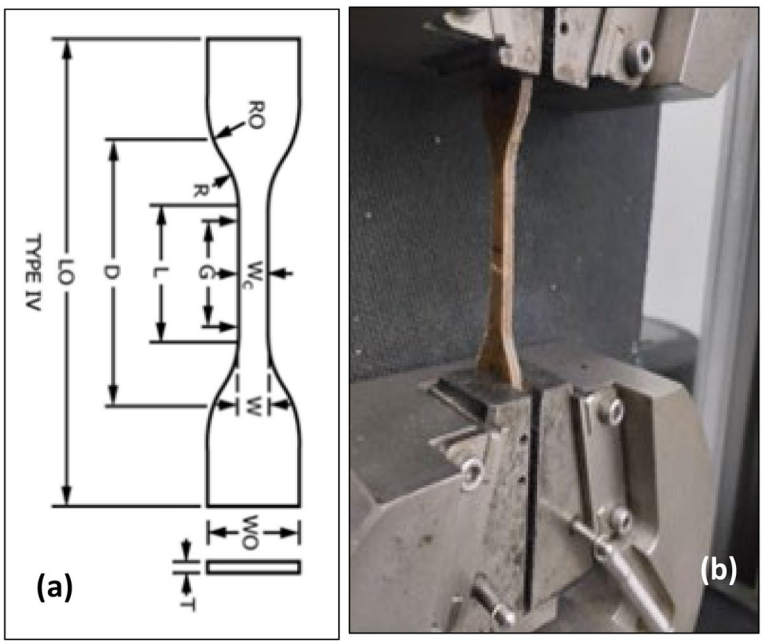

Fig. 3 Tensile test specimen: (**a**) specimen diagram in the ASTM standard, (**b**) Test specimen on the Instron tensile test equipment

Table 2 Dimensions of tensile test specimen (Type IV)

Dimension	Description	Value
LO	Overall length (min): mm	≥ 115.0
D	Distance between grips: mm	65.0 ± 5.0
L	Length of narrow section: mm	33.0 ± 0.5
G	Gage length: mm	25.0 ± 0.13
WO	Overall width: mm	19.0 ± 6.4
W	Width of narrow section: mm	6.0 ± 0.5
RO	Outer radius: mm	25.0 ± 1.0
R	Radius of fillet: mm	14.0 ± 1.0
T	Thickness: mm	3.2 ± 0.4

ASTM D256-10, the impact velocity was 3.8 m/s and the frequency range was 30–100 kHz.

Thermal characterisation

Hybrid and nanoclay hybrid polyamide biocomposites were ground into fine particles, and thermo-gravimetric analysis (TGA) was conducted to measure the weight loss of the hybrid and nanoclay hybrid polyamide biocomposites as temperature were varied. The test was conducted under a controlled nitrogen atmosphere at a flow rate of 50 ml/min, with thermal scans ranging from 25 °C to 600 °C at a heating rate of 10 °C/min. The TGA measurements were performed using a TGA Q500-1660, Waters TA Instruments, USA. This controlled atmosphere ensured oxidative degradation was prevented, allowing the measurement to reflect pure thermal decomposition behavior of the composite constituents. Approximately 10 mg of each sample was used per run in accordance with ASTM E1131-20 [28]. The purpose was to study how much the composite constituents decomposed with the temperature thereby evaluating the thermal stability of the composite and its fraction of volatile components.

Chemical characterisation

Fourier transform infrared spectroscopy analysis The composite board of size 10 mm × 2 mm × 3.2 mm was prepared for Fourier transform infrared spectroscopy (FTIR) analysis. The FTIR test was conducted by using Nicolet IS10-1810, Thermo.Scientific, USA. The spectra were recorded in the range of 400–4000 cm^{-1} with the resolution of 4 cm^{-1}. The purpose of FTIR test was to observe the change of functional groups (if any) because of nanoclay addition.

Morphological characterisation

Scanning electron microscopy test The microstructures of composite specimen, particularly the surface of the fracture, were sputter coated with gold (Au) prior to its scanning by utilising the cold-field-emission scanning electron microscopy (SEM) (JOEL JSM 6400 SEM, JEOL

Ltd., Japan), coupled with energy-dispersive X-ray spectroscopy over the voltage range 5–20 kV at the Institute of Tropical Forestry and Forest Product (INTROP), and Institut Biosains (IBS), both in Universiti Putra Malaysia.

Results

Water absorption

The water absorption results for hybrid polyamide biocomposites with 0 wt.% nanoclay content demonstrate a direct association between hybrid content and water uptake, as illustrated in Fig. 4. Incorporating a fibre content of 20–50 wt.% enhances the water absorption capacity of the hybrid composite by over 130%. The elevated hybrid content intrinsically enhances the material's natural fibre hydrophilic characteristics, presumably due to the augmented presence of polar groups in the hybrid component [22, 29, 30]. In similar research using more percent of mineral filler, there is slight increase in the level of water absorbed, which is consistent with the hydrophilic nature of mineral materials [29–31].

The introduction of nanoclay content significantly impacts water absorption behavior, particularly evident in the transition from 0 to 3% nanoclay content. nanoparticles dispersed in the polymer matrix could lower the water absorption of the composites and improve their performance in humid environments [32]. The 50% hybrid composition showed a significant reduction of up to 17%, while maintaining the highest absorption among all compositions. Similarly, all other hybrid compositions exhibit reduced water absorption at 1% nanoclay, with reductions ranging from 15–30% compared to the hybrid composites. This trend continues with increasing nanoclay content up to 3%, though the rate of reduction diminishes. Hybrid nanocomposites can suppress water absorption by adding nanoclay, which reduces void content, creates a moisture barrier, and limits polymer chain motions and relaxation [33, 34].

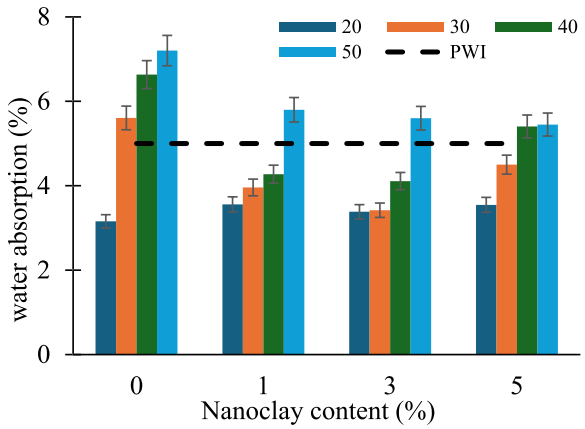

Fig. 4 Water Absorption of hybrid polyamide biocomposites with different NC contents

The role of nanoclay as a barrier material becomes evident through the consistent reduction in water absorption across all compositions. This can be attributed to the creation of a tortuous path by the dispersed nanoclay particles, which impede water molecule diffusion through the composite matrix. The platelike structure of nanoclay particles forces water molecules to navigate a longer, more complex path through the material, effectively reducing the overall water absorption rate [34, 35]. However, at 5% nanoclay content, a slight increase in water absorption is observed across all compositions, suggesting that higher clay concentrations may lead to agglomeration and create additional pathways for water penetration.

When compared to the Permanent Way Institution (PWI) final technical report 5% water absorption [36], the results show that compositions with 20% and 30% hybrid content consistently meet this requirement across all nanoclay concentrations. The 40% and 50% hybrid compositions initially exceed the PWI standard at 0% nanoclay but achieve compliance with the addition of 1% or more nanoclay content. This demonstrates that nanoclay incorporation effectively brings the water absorption properties within acceptable industry standards, particularly for compositions with higher hybrid content that would otherwise exceed the requirement. Here, the optimal balance appears to be achieved at 3% nanoclay content, where all compositions show stable water absorption below or near the PWI threshold while maximising the barrier effect of the nanoclay.

The integration of nanoclay demonstrates a crucial barrier effect, optimally at 3 wt.%, significantly mitigating water absorption by creating a tortuous diffusion pathway, thereby enhancing composite resilience in humid conditions. However, surpassing this optimal concentration triggers particle agglomeration, inadvertently compromising the composite integrity by facilitating additional water ingress pathways.

Mechanical properties

Flexural strength

The flexural strengths and modulus of elasticity of nanoclay hybrid kenaf/glass biocomposites at various concentrations were shown in Fig. 5a. For all samples (20-50wt.%), hybrid treated kenaf/glass reinforced biocomposite showed a 31% rise in flexural strength (68.4 MPa—89.5 MPa). The increase in flexural strength indicates that the kenaf and polymer matrix have adhered successfully. This is because of the kenaf surface treatment, earlier reported in [24, 37]. Consequently, resulting

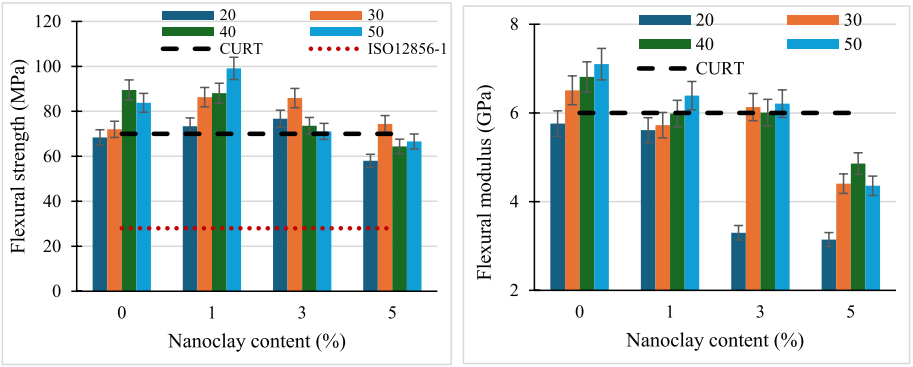

Fig. 5 Flexural properties of hybrid polyamide biocomposites with different NC contents: (**a**) flexural strength, (**b**) flexural modulus. CURT, Standards of China Urban Rail Transit. ISO 12856–1, Plastic railway sleeper material characteristics for railway application

in the improved stress transfer under service loading during testing. Thus, aligning in findings to those of [37] and [24] indicating a favourable interfacial interaction (see Fig. 10f and g) between the treated kenaf and polyamide matrix. Furthermore, when kenaf was alkalised, the available hemicellulose and lignin on its surface were removed by the sodium hydroxide (NaOH) solution treatment. Absence of these ingredients results in a larger and rougher surface area, thereby enhancing the interlocking between the fibre and matrix [38, 39].

At 0% nanoclay content, the 30%, 40% and 50% hybrid compositions exhibit the highest flexural strengths of approximately 72 MPa, 90 MPa and 84 MPa respectively, significantly exceeding both the Standards of China Urban Rail Transit (CURT) standard (70 MPa) and ISO 12856–1 [40] standard (28 MPa). The addition of 1% NC content shows notable improvements, particularly for the 30% and 50% hybrid compositions, with the 50% composition reaching peak strength of about 95 MPa, representing a 36% and 240% increase above CURT and ISO 12586 respectively. However, further increases in NC content to 3% and 5% lead to progressive deterioration in flexural strength across all compositions, with the 5% nanoclay content resulting in values falling below the CURT standard, particularly for the 20% hybrid composition which drops to approximately 58 MPa.

The flexural strength analysis reveals that optimal performance is achieved at 1% nanoclay content, suggesting this concentration provides the best balance of particle dispersion and matrix reinforcement. The 30% hybrid composition demonstrates the most consistent performance across varying nanoclay contents, maintaining values above the CURT standard until 5% nanoclay content. The significant decrease in strength at 5% nanoclay content across all compositions indicates a potential threshold where particle agglomeration begins to compromise the material's structural integrity, resulting in deteriorating mechanical properties.

Three distinct forms of reinforcement influence stress transfer. The initial treatment of kenaf fibre created a favorable bond with matrix, while stress transfer between kenaf and glass fibre remained significant. If filler matrix adhesion is inadequate, the filler cannot carry external loads, resulting in no improvement in flexural strength beyond that of the matrix alone [41, 42]. Increasing the concentration of nanoclay can lead to agglomeration, resulting in poor dispersibility within the polyamide matrix. This also raises the viscosity of the polymer matrix, which in turn increases internal porosity and reduces flexural strength [43, 44]. Higher filler content concentrates stress on the agglomerated nanoclay, promoting crack propagation through the composite. A similar trend was observed in nanocellulose biocomposites filled with 2.5% to 50% nanoclay, where flexural strength gradually decreased up to 10% concentration before significantly deteriorating beyond that point [45].

Flexural modulus

As shown in Fig. 5(b), the incorporation of hybrid fibres (natural and synthetic) 20–50% considerably enhances the flexural modulus of the composite ranging between 6–7 GPa. As the kenaf/glass fibre increases in the range of 20–50%, the overall flexural modulus of the hybrid increased meeting the standard (6 GPa) stipulated by the Ministry of Housing and Urban–Rural Development of the Peoples's Republic of China (Mohurd). This conformation is mainly because of the synergistic role of both fibres as the skeleton of the matrix, thereby improving the flexural modulus of the matrix due to the removal of hemicellulose and lignin on the natural fibre's surface by

the NaOH solution resulting in the rougher surface area. It could be responsible for the formation of some troughs on the fibre. The increase in fibre surface area might increase the matrix penetration and wetting onto the rough surface of the fibre which results in the enhanced interfacial bonding within the composite [46].

The addition of nanoclay (1–3%) showed a negligible showed a negligible effect on the flexural modulus. However, at higher nanoclay concentration 5wt.%, a significant decline in the composites flexural modulus was seen. Agglomeration of a greater quantity of nanoclay within the polymer matrix occurs because of their high surface area, thereby attracting other neighbouring clays. During the bending test, load was first applied to the matrix (by right) before transferring the stress to the nanoclay. Here, nanoclay had filled the polymer matrix, probably resulting in an uneven of the composite which would lead to inadequate stress transfer. Voids serving as crack initiation points are formed by the agglomeration of the nanoclay (see E3-3, Fig. 11). Therefore, an insufficient dispersion of the nanoclay within the polymer matrix will cause degradation of the composite's overall properties and performance [47–49]. Furthermore, it had been reported elsewhere that the addition of nanoclay at higher concentration results in a decrease of flexural modulus [24, 50].

Firstly, other reasons for the flexural modulus decrease could be because of the anisotropic behaviour (compression and tension) displayed by the composite during bending test [51]. Secondly, it could be because of the hybrid reinforcement with fibres and nanoclay which could greatly disrupt the viscosity of the polymer matrix as well as its properties [52]. Thirdly, the nano-hybrid composites with its different reinforcing materials could experience multiple fibre breakage during testing at the time load was continuously applied. The natural (kenaf) fibre is likely to first give way (break) because the synthetic (glass) fibre is known for superior strength than natural fibres [53]. Despite the kenaf fibre breakage, the composite continues to sustain the applied load without any sign of degrading because of the presence of the glass fibre within the composite which continues to support the load after the breakage of the kenaf fibre, until the glass fibre breaks. This indicates the synergistic behaviour as displayed by the hybrid in its ability to transfer of stresses [54, 55].

To this end, the presence of nanoclay further increases the uncertainties of the composite flexural strength, being a measure of the change in transfer of stress from particle to fibrous materials. Here, the transfer of stress could have primarily occurred between nanoclay and hybrid fibres because of its insufficient adhesion with the polymer matrix. The 30–50% composition maintains relatively stable performance around 6–7 GPa throughout the nanoclay content range, while the 20% composition shows a declining trend with increasing nanoclay content. This suggests that applications requiring high stiffness might benefit from higher hybrid and nanoclay contents, while those prioritizing strength should maintain lower nanoclay concentrations around 1–3%.

In contrast to some literature, the flexural strength of the composite was significantly improved by the inclusion of high strength and alkali free glass fibre, which maintained its rigidity due to its chopped strand form with optimal dimensions. During mixing, nanoclay and PA6 were added first, followed with glass GF and TKF at the final stage, minimising shear effects. This method preserved fibre length, ensured a high length to diameter (L/D) ratio, and promoted uniform dispersion in the matrix. The result was enhanced reinforcement efficiency and improved mechanical performance of the composite.

The composite sample E3-2, comprising 30% hybrid fibre reinforcement (10wt.% TKF and 20wt.% GF) along with 3wt.% nanoclay in a 70wt.% PA6 matrix, displayed notable mechanical and physical performance. It achieved a flexural strength of 85.9 MPa, a flexural modulus of 6.13 GPa, tensile strength of 43.1 MPa, tensile modulus of 6.9 GPa, impact toughness of 28.24 kJ/m^2, and water absorption of 3.42%. These values clearly outperform many traditional and emerging composite materials. When compared to conventional concrete, geopolymer concrete, steel fibre-reinforced geopolymer concrete, and particulate-filled resins with hybrid steel fibres, which exhibit lower flexural strengths of 5.67 MPa, 6.17 MPa, 8.42 MPa, and 22 MPa respectively [56, 57], sample E3-2 offers a distinct mechanical advantage.

Additionally, sample E3-2 surpasses the performance benchmarks established by both ISO 12856–1 [40] and fibre foamed Urethane (FFU) standards for railway applications. The flexural strength exceeds the ISO minimum of 28.0 MPa by 206%, and the FFU standard of 70.0 MPa by 23%, highlighting its suitability for structural functions such as railway sleepers. The results affirm that increasing the hybrid fibre content (TKF/GF) generally leads to enhanced mechanical performance, in line with the rule of mixtures principle, and findings from [58] and [12], which establish that higher proportions of stiff reinforcements improve composite stiffness. However, a give and take exists, as increased reinforcement content can also elevate brittleness, necessitating a balanced formulation for practical applications.

Flexural strength and impact toughness observed in this study were further benchmarked against various hybrid composites from prior literature. The flexural performance of E3-2 exceeds that of epoxy polymer/crumb rubber composites (23.12 MPa), epoxy polymer/PP fibre

(30.66 MPa) [59], and RHDPE/Calcium Carbonate composites (20.4 MPa) [31]. Nevertheless, it remains below the flexural strengths recorded for higher performing composites such as RHDPE/glass fibre/PP/compatibiliser (167.80 MPa) [12] and epoxy hybrid glass/kenaf/nanoclay composites (152.0 MPa) [24] as summarised in Table 3. These comparisons substantiate the high but not peak performance level of E3-2 in the broader context of composite development.

Overall, the mechanical evaluation confirms that the nanoclay hybrid PA6 biocomposite meets international plastic sleeper standards, qualifying it for railway infrastructure deployment. While it does not match the flexural strength of the high grade composites, its performance clearly surpasses several benchmark and standard materials, including the ISO 12856–1 minimum and FFU standard. The balanced integration of TKF/GF, and nanoclay into a PA6 matrix presents a strong, durable, and industrially relevant solution. These findings collectively affirm the potential of E3-2 as a structurally reliable composite, demonstrating that properly engineered biosynthetic hybrids can serve as effective materials for high performance applications in rail transport systems.

The incorporation of 1 wt.% nanoclay synergistically enhances flexural strength and modulus by promoting effective fibre-matrix stress transfer, while exceeding this limits initiates particle agglomeration that could be detrimental. These affirms the critical importance of controlling nanofiller dispersion and hybrid fibre proportions to maximise structural integrity and durability for advanced composite applications.

Tensile stress

The tensile strength results shown in Fig. 6(a) demonstrate a clear declining trend with increasing nanoclay content across all hybrid compositions. At 0% nanoclay content, the 30% hybrid composition exhibits the highest tensile strength of approximately 55 MPa, followed closely by 20% composition at 52 MPa. The addition of 1% nanoclay content results in a moderate decrease, with values ranging from 42–48 MPa across all compositions, representing a 10–15% reduction from baseline values.

Table 3 Comparison of the flexural strength of composite in published literature with E3-2

Specimen	Flexural strength (MPa)	Reference
E3—2*	85.9 ± 0.05	present study
RHDPE/glass fibre/PP/compatibiliser	167.80 ± 0.05	[12]
RHDPE/Calcium carbonate	20.4 ± 0.05	[31]
Epoxy hybrid glass/kenaf/nanoclay composite	152.0 ± 0.05	[24]
Epoxy polymer/crumb rubber	23.12 ± 0.05	[59]
Epoxy polymer/PP fibre	30.66 ± 0.04	[59]
FFU	70.00 ± 0.05	[60]
Other composites	21.45 ± 0.05	[61]
Plastic railway sleeper material characteristics for railway applications (railroad ties)	28.0 ± 0.05	[40]

E3-2: E stands for hybrid batch E, 3 stands for 30% hybrid (i.e., 10 Treated kenaf fibre, and 20% glass fibre), while 2 stands for second nanoclay addition (i.e., 3%). The remaining percentage for the polyamide six matrix

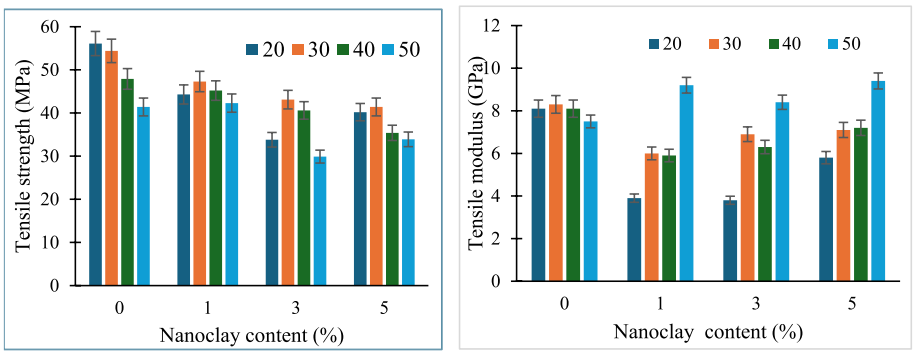

Fig. 6 Tensile properties of hybrid polyamide biocomposites with different NC contents: (**a**) tensile strength, (**b**) tensile modulus

Further increases in nanoclay content to 3% and 5% lead to more significant decreases, with the most pronounced drop observed in the 50% hybrid composition at 3% nanoclay, showing approximately a 45% reduction from its initial value. The 20% hybrid composition consistently shows the lowest tensile strength at higher nanoclay contents.

Analysis of the tensile strength results indicates that the incorporation of nanoclay has a predominantly negative effect on the material's ultimate strength. The consistent decline across all compositions suggests that nanoclay particles may be acting as stress concentrators or creating weak interfaces within the matrix, leading to premature failure. The most significant deterioration occurring between 0 and 3% nanoclay content points to a critical concentration range where the material's load-bearing capacity is most compromised, with relative stability observed between 3 and 5% nanoclay content, albeit at lower strength values.

The tensile modulus trends illustrated in Fig. 6(b) reveal a contrasting behavior, particularly for the 50% hybrid composition. At 0% nanoclay, all compositions show similar modulus values of approximately 8 GPa. However, with increasing nanoclay content, the 50% composition demonstrates significant improvement, reaching peak values of about 9.5 GPa at 1% nanoclay (representing an 18% increase) and maintaining elevated values through 5% nanoclay content. Conversely, the 20% composition shows a substantial decline, dropping to approximately 4 GPa at 1% and 3% nanoclay contents, representing a 50% decrease.

The tensile modulus behavior reveals that while higher nanoclay contents may compromise strength, they can enhance the material's stiffness, particularly in higher hybrid compositions (50%). This dichotomy suggests that the nanoclay particles effectively restrict polymer chain mobility, increasing stiffness, but may simultaneously create discontinuities that reduce ultimate strength. The recovery in modulus observed at 5% nanoclay content for some compositions indicates a possible secondary reinforcement mechanism at higher clay concentrations, though this benefit is offset by the corresponding reduction in tensile strength**.** Notably, increasing nanoclay concentrations has compromised tensile strength across all hybrid compositions, highlighting the role of nanoclay as stress concentrators and interfacial disruptors. Conversely, increased tensile modulus in high hybrid compositions at moderate nanoclay inclusion (1–5%) indicates beneficial stiffening effects through constrained polymer chain mobility, aligning the critical balance required between stiffness enhancement and strength preservation.

Impact toughness

The impact toughness of polyamide biocomposites is significantly influenced by the content and composition of hybrid fibres as shown in Fig. 7. Increasing the content of hybrid fibre from 20% (E2) to 30% (E3) enhances the impact toughness, with E3 composites achieving a peak value of 31.2 kJ/m^2 being approximately 4% close to that of the fibre-reinforced foamed urethane (FFU) products (32.40 kJ/m^2) used in the Chinese railway system. This

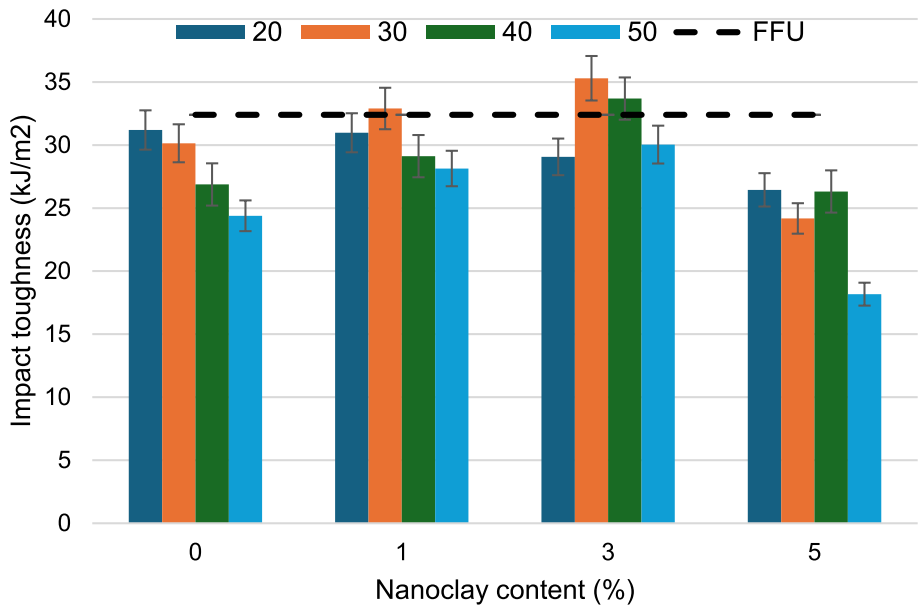

Fig. 7 Impact toughness of composite at different hybrid fibre and nanoclay content

improvement is attributed to the balanced reinforcement effect provided by the hybrid combination of TKF/GF, which offers an effective synergy between stiffness, energy dissipation, and interfacial bonding with the polyamide matrix [12].

However, further increasing the fibre content beyond 30%, as observed in E4 (40%) and E5 (50%), leads to a decline in impact toughness. This reduction is attributed to matrix saturation, fibre agglomeration, and poor dispersion at higher hybrid fibre loadings, which hinder stress transfer and promote premature failure. These findings are consistent with previous studies emphasizing the importance of maintaining optimal fibre volume fractions to balance reinforcement benefits and matrix continuity [57, 62]. Additionally, a reduction in impact toughness is a common phenomenon in plastics, particularly those with high strength, such as those reinforced with hybrid kenaf/glass (TKF/GF) fibres in a PA6 matrix. The inclusion of TKF/GF enhances the stiffness of the composite and contributes to heterogeneous nucleation, thereby increasing the crystallinity of the matrix. However, higher crystallinity reduces the material's deformation ability and consequently diminishes its impact strength. Furthermore, while a strong bond between the matrix and TKF/GF fibres facilitates effective stress transfer under tensile loading thereby resulting in enhanced tensile strength. Additionally, it restricts crack propagation under impact loads. As a result, the impact energy is not effectively absorbed, leading to a further reduction in impact toughness [59].

The incorporation of nanoclay further modifies the impact performance of these composites. At low nanoclay content (1wt.%), marginal improvements in impact toughness were observed, particularly in E2-1 and E3-1. The limited reinforcement effect at this level may arise from suboptimal nanoclay dispersion or insufficient interfacial interaction. Remarkably, the introduction of 3% nanoclay results in a significant increase in toughness across all hybrid systems, with E3-2 composites reaching approximately 36 kJ/m^2, surpassing the Chinese railway system fibre reinforced foamed urethane (FFU) product reaching (32.40 kJ/m^2) as shown in Fig. 7. This enhancement suggests that nanoclay content at this concentration is well dispersed within the matrix, promoting mechanisms such as crack deflection, crack pinning, and increased fibre matrix adhesion. These mechanisms collectively contribute to energy dissipation during impact loading. Similar observations have been reported in the literature, where nanoclay platelets improved the mechanical performance of fibre reinforced polymers by reinforcing the matrix and delaying crack propagation [63, 64].

Nevertheless, at a higher nanoclay content of 5wt.%, there is a consistent reduction in impact toughness across all hybrid fibre composites, with the E5 composite showing the most severe decline to approximately 26 kJ/m^2. The negative effect at this loading is attributed to nanoclay agglomeration, which induces stress concentration zones, matrix embrittlement, and inhomogeneity in the microstructure. These defects impair the load-bearing capability of the matrix and diminish the reinforcing potential of both the nanoclay and fibres. Excessive nanoclay content has been previously shown to compromise toughness and ductility, especially in hybrid composites where the matrix-fibre-nanoclay interfacial balance is delicate [63].

In summary, the results obtained demonstrate that both hybrid fibre ratio and nanoclay content play critical roles in optimising the impact performance of polyamide six composite. An optimal fibre hybrid content of 30% (E3) yields superior toughness due to the well balance contribution of TKF/GF to load transfer and energy absorption. Concurrently, the incorporation of 3% nanoclay further enhances this effect, likely through improved interfacial bonding and crack resistance mechanisms. Although, any deviations from these optimal values (either by increasing fibre content or nanoclay concentration) result in diminished mechanical performance due to fibre saturation or nanoclay agglomeration. To this end, these findings support the hypothesis that a synergistic balance between fibre reinforcement and nanofiller dispersion is essential for maximising the toughness of hybrid fibre reinforced nanocomposites.

The strategic integration of 3 wt.% nanoclay jointly elevates impact toughness beyond industrial benchmarks, signifying optimal dispersion, enhanced crack resistance, and improved fibre-matrix interfacial interactions. However, surpassing this critical concentration level will compromises mechanical resilience due to nanoclay agglomeration and structural heterogeneity, signifying the delicate interplay required for maximised energy absorption performance.

Thermal properties

Thermogravimetric analysis (TGA)

The TGA and DTG curves of nanoclay hybrid polyamide biocomposite are shown in Fig. 8. The loss of physically bound or interlayer water for polyamide six composite is mainly between 40–275 °C and, to a lesser extent, low-molar-mass extractables [65]. The increase in weight loss shown in Table 4 at a temperature range up to 300 °C is about 2% (0.12% to 1.81%). The higher figures recorded for the most highly loaded formulations (E3 and E5) reflect the greater number of hydrophilic silicate galleries able to trap moisture. Similar trends have been reported

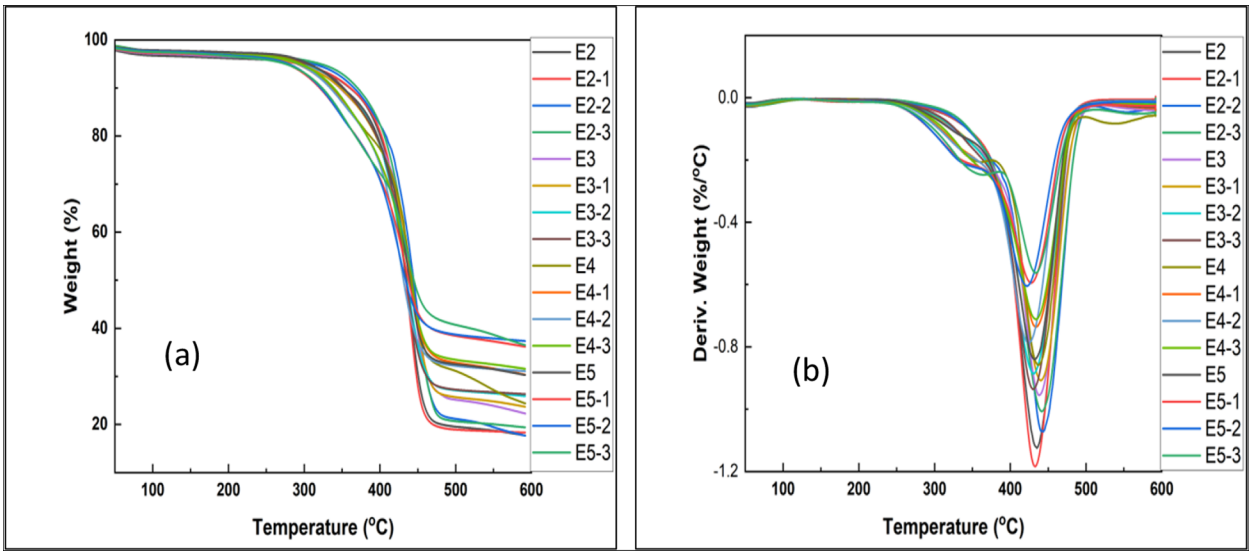

Fig. 8 (**a**) TGA, and (**b**) DTG curves of nanoclay hybrid polyamide biocomposite

Table 4 Weight loss (WL) of hybrid polyamide bicocomposite with various nanoclay loadings

Sample Id	240 -T_{onset}°C (W_L (%))	T_{onset} - T_{endset}°C (W_L (%))	T_{onset} °C	T_{endset}°C	Residue (%)
E2	0.12	75.17	254.16	464.39	17.73
E2-1	0.22	74.22	256.57	458.42	18.33
E2-2	0.71	74.72	285.82	483.12	17.72
E2-3	0.75	73.12	294.21	471.15	19.42
E3	1.34	69.63	295.46	481.33	22.64
E3-1	1.01	68.43	285.37	471.02	23.98
E3-2	1.16	66.47	291.66	465.12	26.16
E3-3	1.35	66.07	296.60	461.94	26.60
E4	0.74	68.94	276.92	542.85	24.38
E4-1	0.19	63.75	254.04	485.50	30.35
E4-2	0.27	63.02	257.84	463.51	31.09
E4-3	0.21	62.57	254.24	475.23	31.58
E5	1.81	64.57	300.76	549.13	30.28
E5-1	0.70	59.55	266.54	573.42	36.18
E5-2	0.68	58.61	266.46	565.01	37.36
E5-3	0.45	59.31	259.67	582.28	36.50

for PA-6/montmorillonite nanocomposites, where the first DTG shoulder scales with clay content [65].

The addition of nanoclay obviously delays the start of degradation by 10–40 °C relative to the hybrid composite (E2 to E2-3 and E4-1 to E4-3). This shift supports the barrier effect where the exfoliated silicate platelets create a tortuous path that slows oxygen diffusion and volatile escape resulting in suppressing radical chain scission at the surface of the composite [66]. Interestingly, T_{onset} does not consistently increase with residue yield. For instance, E5-1 to E5-3 records higher char (36–37%) but with a slight decrease in T_{onset} (266 to 260 °C). This crossover signifies competition between kinetic stabilisation and catalytic effects of iron or sodium traces in organoclays, which can accelerate amide pyrolysis once the optimum loading of the nanofiller is exceeded [67].

The total mass loss 59% –75% between T_{onset} and T_{endset}, corresponds to the random chain scission of the polyamide backbone and volatilisation of ε-caprolactam and cyclic oligomers. The width of T_{endset} broadens when well-dispersed clay is present (E4 and E5 series), indicating a distributed degradation pathway rather than a single kinetic process.

From Table 4, residue rosed from 17.7% to 37.36% (E2, E5-2) as clay content increases, in excellent agreement with the formation of an inorganic–carbonaceous char documented in PA/nanoclay systems [68]. This char layer shields the underlying polymer, further lowering the maximum mass-loss rate as the peak temperature shifts from 451 °C to 411 °C for E2-3 and E5-2 and further explaining the smaller change in mass values in the E5 series.

The systematic evolution of T_{onset} and T_{endset}, segmental weight loss and residue across the E2–E5 series confirms that nanoclay acts through a combined barrier/char mechanism. Optimal loadings E2-E3 series maximise the thermal-stability envelope, whereas excessive clay E2-3, E3-3, E4-3 and E5-3, sacrifices onset temperature despite higher char formation. These insights

provide a quantitative basis for tailoring hybrid polyamide biocomposites for high-temperature or flame critical applications.

Considering the E3-2 formulation having 292 °C onset temperature, showed approximately a 40 °C of processing headroom over typical PA6 melt temperatures (approximately 250 °C), so E3-2 can be extruded or injection-moulded without need for special precautions. In compared with E3-3, the T_{onset} is only 5 °C lower, yet the T_{endset} is reached 15 °C earlier, indicating that the main scission/volatilisation sequence completes faster. This kind of behaviour is often attributed to partially intercalated rather than fully exfoliated clay galleries, which shorten the diffusion path for volatiles and act as nanoreactors that accelerate the latter half of degradation [69].

In addition, at 26% residue, E3-2 outperforms both E3 (22.6%) and E3-1 (24.0%), confirming that its clay loading is high enough to generate a coherent silicate-rich char that shields the melt. The char rise, which is about 4%, is proportionally larger than the decrease in onset between 4 °C and E3. Therefore, the char per onset temperature efficiency is highest for E3-2 in this set.

Hence, E3-2 strikes a balanced middle ground by yielding a robust 26% char for condensed-phase flame inhibition and maintains a comfortable margin of processing window of about 40 °C. Uptake of moisture was kept low, which aids drying and dimensional control. For general flame retardant or electrically insulated PA components such as connector housing, LED back shells that will generally not be prolonged above 260 °C in service. E3-2 is an economical yet thermally robust choice. If peak oxidative stability is paramount, E3-3 (or the E5 family) remains superior; yet for a cost-performance compromise, E3-2 compares favourably with widely reported 5–7 wt% nanoclay benchmarks that raise Tonset by about 25 °C and boost char by 3 to 5 wt% in PA6 matrices [70].

Nanoclay incorporation strategically increases thermal stability and char yield through collective barrier and catalytic char-forming mechanisms, significantly extending the processing and service temperature windows of polyamide composites. However, exceeding the optimal nanoclay content initiates accelerated pyrolysis, underlining the necessity of precise filler dispersion to balance thermal resilience with processability for advanced thermal management applications.

Chemical properties

Fourier transform infrared spectroscopy (FTIR) analysis

The FTIR spectra of hybrid polyamide biocomposite containing various dosages of nanoclay particle concentrations is shown in Fig. 9, by which the change in functional groups can be clearly identified. Table 5 shows the functional groups and the respective possible assignments for each peak position. The O–H stretching vibration and hydrogen bonding of hydroxyl groups are represented by the peak at 'a' (between 3400 to 3200 cm^{-1}). These are ascribed to both intramolecular and intermolecular hydrogen bonding as well as free OH groups [71]. The main component of this band is the superposition of structural silanol -OH groups from montmorillonite and surface hydroxyls from treated kenaf fibre (TKF) cellulose. The peak intensity rises approximately linearly as the TKF content rises (5 to 20 wt.%) because of the increasing contribution of free -OH groups from the cellulose surface [72]. Structural silanol OH groups are introduced by the gradual addition of montmorillonite

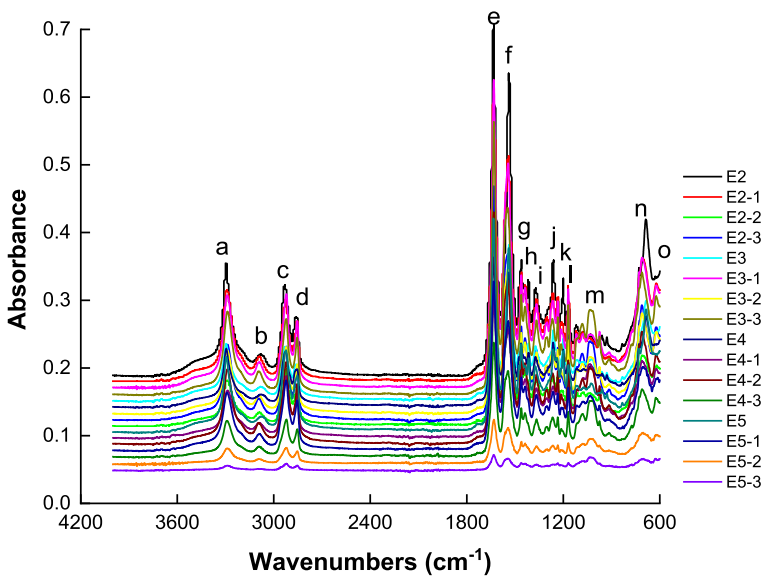

Fig. 9 FTIR Spectra of hybrid and nanoclay hybrid polyamide biocomposites

Table 5 FTIR spectral data for nanoclay hybrid polyamide biocomposites

Peak Label	Wavelength (cm^{-1})	Peak positions																Possible Assignment
		E2	E2-1	E2-3	E2-2	E3	E3-1	E3-2	E3-3	E4	E4-1	E4-2	E4-3	E5	E5-1	E5-2	E5-3	
a	3400–3200	3296	3292	3292	3287	3296	3290	3289	3288	3295	3286	3289	3291	3295	3291	3288	3286	O–H stretching vibration (hydrogen-bonded hydroxyl)
b	3000–2850	2932	2924	2922	2922	2931	2921	2922	2923	2928	2922	2923	2921	2924	2923	2922	2921	C–H stretching vibration in cellulose and hemicellulose (asymmetric $–CH_2$/$–CH_3$)
c	2900–2800	2861	2855	2854	2854	2861	2854	2855	2855	2855	2854	2855	2854	2854	2855	2854	2854	C–H stretching (symmetric $–CH_2$/$–CH_3$)
d	1680–1600	1634	1633	1631	1632	1635	1633	1632	1632	1634	1633	1632	1632	1633	1633	1631	1633	Amide I (C=O stretch of PA6), absorbed moisture
e	1550–1475	1538	1541	1541	1545	1538	1542	1545	1546	1537	1542	1545	1545	1538	1541	1541	1545	Amide II (N–H bend + C–N stretch), aromatic C=C stretching in lignin
f	1470–1450	1462	1461	1461	1461	1462	1461	1461	1461	1462	1461	1461	1461	1462	1461	1460	1461	C–H bending (methylene scissoring)
g	1450–1400	1417	1436	1436	1436	1417	1436	1436	1436	1416	1436	1436	1436	1416	1436	1436	1436	O–H in-plane bending
h	1380–1350	1372	1366	1366	1366	1373	1366	1366	1366	1373	1367	1366	1366	1374	1367	1365	1366	Amide III / N–O symmetric overlap
i	1280–1250	1263	1265	1264	1268	1262	1265	1267	1268	1263	1263	1267	1267	1262	1264	1265	1266	C–N stretching (aromatic amine)
j	1220–1190	1201	1213	1213	1214	1201	1213	1213	1213	1201	1213	1213	1213	1201	1212	1213	1213	C–O / Si–O stretching (ester / Si–O–Si)
k	1180–1150	1170	1169	1169	1169	1170	1169	1169	1169	1169	1169	1169	1169	1169	1169	1169	1168	Aromatic C–H in-plane bending
l	1130–1090	1121	1120	1119	1101	1117	1119	1118	1101	1116	1101	1101	1101	1116	1115	1101	1101	Aromatic C–H in-plane bending
m	720–700	709	710	710	711	709	710	711	711	709	711	711	711	709	709	710	713	Aromatic C–H out-of-plane bending
n	710–670	687	707	707	707	685	707	707	707	684	707	707	707	684	707	703	700	Aromatic C–H out-of-plane bending
o	590–560	576	580	580	580	576	583	586	580	576	581	580	583	576	579	589	577	Ring skeletal deformation

at 1, 3, and 5 weight percent, which causes a discernible shoulder between 3600 and 3400 cm^{-1}. this is due to the increased interactions of hydrogen bonding between cellulose and the Si–OH groups of the clay, this broadens and strengthens the whole band [73, 74].

The peaks at 'b' and "c" (between 3000—2850 cm^{-1}) reflect the C–H stretching vibrations of methyl ($–CH_3$) and methylene ($–CH_2$) groups. These vibrations are mostly derived from PA6 chains, with a small contribution from the cellulose matrix [75]. These peaks display a distinctive doublet, the overall intensity of which drops because the mass fraction of PA6 drops (80–50 wt.%) resulting in the decrease of all peak height ratio (between 2932–2860) for all sample. Due to its inorganic nature and absence of aliphatic C–H groups, nanoclay has little to no effect on these bands [75]. Therefore, any spectrum attenuation in this region is directly related to the decrease in PA6 content.

The peak at 'd' (centered around 1634 cm^{-1}) represents the stretching vibration of the carbonyl group (C=O) associated with the amide I band of polyamide 6 (PA6) [75]. This band gradually decreases in intensity as the PA6 content is reduced. Upon addition of 0–5 wt. % montmorillonite, a small red shift of approximately 1–4 cm^{-1} is observed, along with band broadening. These changes indicate hydrogen bonding between the amide C=O groups and the –OH or –O–Si functional sites within the silicate clay galleries, suggesting partial intercalation or exfoliation of PA6 chains within the clay layers [75, 76].

The peak at 'e' (1538 cm^{-1}) corresponds to the Amide II band, primarily arising from N–H bending and C–N stretching vibrations in PA6. This band shows a progressive decrease in intensity as the PA6 content is reduced, mirroring the behavior of the Amide I band. However, with the addition of montmorillonite clay, the Amide II peak broadens noticeably, reflecting enhanced hydrogen bonding between the N–H groups of PA6 and the O–Si groups within the silicate layers. The resulting increase in the Amide II to Amide I intensity ratio is a spectral marker of stronger polymer–clay interactions [77, 78].

The peaks from 'f' to 'h' (between 1462–1372 cm^{-1}) represent overlapping vibrational modes affected by compositional changes. The CH_2 scissoring band at 1462 cm^{-1} diminishes with decreasing PA6 content, while the cellulose-associated O–H bending vibration at 1416 cm^{-1} intensifies as the TKF fraction increases [72]. Near 1372 cm^{-1}, a composite band attributed to Amide III, N–O, and CH bending broadens in the presence of clay, reflecting reduced polymer chain mobility within the constrained clay matrix [72].

The peaks from 'I' to 'l' (1263, 1201, 1170, and 1121 cm^{-1}) correspond to overlapping C–N and C–O stretching vibrations from PA6 and cellulose, respectively, along with contributions from Si–O–Si stretching. While these bands are only marginally affected by the

TKF content, they intensify significantly with increasing nanoclay loading. This is due to the in-plane Si–O–Si stretch of 2:1 smectite montmorillonite, centered near 1030–1010 cm^{-1}, which overlaps and extends into the 1200–1100 cm^{-1} region. The resulting envelope serves as a sensitive spectral indicator of clay presence and concentration (Shelly et al., [79].

The peaks at 'm' and 'n' (between 729–687 cm^{-1}) correspond to aromatic C–H out-of-plane bending vibrations associated with residual lignin in treated kenaf fibre (TKF). These weak bands increase slightly with rising fibre content but remain unaffected by the addition of nanoclay, which does not contribute to this spectral region [80].

The peak at 'o' (between 590–560 cm^{-1}) corresponds to a skeletal ring and Si–O bending vibration, arising from a combination of aromatic structures in lignin or cellulose and the bending modes of montmorillonite silicate sheets. While this band remains relatively unchanged with varying TKF content, it intensifies consistently with increasing nanoclay, reflecting the contribution of Si–O bending modes [79].

Figure 9 shows that, as TKF adds hydroxyl polar sites, and nanoclay adds both silanol groups and high-aspect reinforcement, the hybrid shows a gradual transformation from a PA6-dominated "amide" spectrum toward a fibre/clay-dominated "hydroxyl-silicate" spectrum. The simultaneous down-shift of amide peaks and up-shift (intensity) of Si–O and O–H bands signal synergistic hydrogen-bond networks between PA6/NC/fibre interfaces, which supports the mechanical improvements typically seen in such hybrids. This is consistent with the finding obtained by Kis et al. [77] and Wu et al [78].

FTIR spectroscopy showed that the strategic incorporation of nanoclay and treated kenaf fibres induces a pronounced shift from polyamide-dominated amide functionalities toward a hydroxyl-silicate network, indicative of robust interfacial hydrogen bonding. This spectral evolution highlights the critical synergy between nanoclay exfoliation, fibre functionalisation, and matrix interactions, which fundamentally showcase enhancing composite integrity and performance.

Microstructures

Scanning electron microscopy (SEM)

The scanning electron micrographs of hybrid composites with varying ratios of treated kenaf fibre (TKF) and glass fibre (GF), ranging from 0 wt.% to 50 wt.% total fibre content, reveal critical morphological features that correlate closely with the mechanical behavior of the materials. In the neat matrix without any fibre reinforcement (Fig. 10 a and b), the surface appears smooth, indicating the characteristic of a homogeneous and brittle fracture. This is consistent with the literature, which attributes such failure in polymer matrices to the absence of stress transfer mechanisms provided by reinforcing fibres [81]. However, the addition of fibres at E2 (5 wt.% TKF and 15 wt.% GF) begins to show interaction between the matrix and

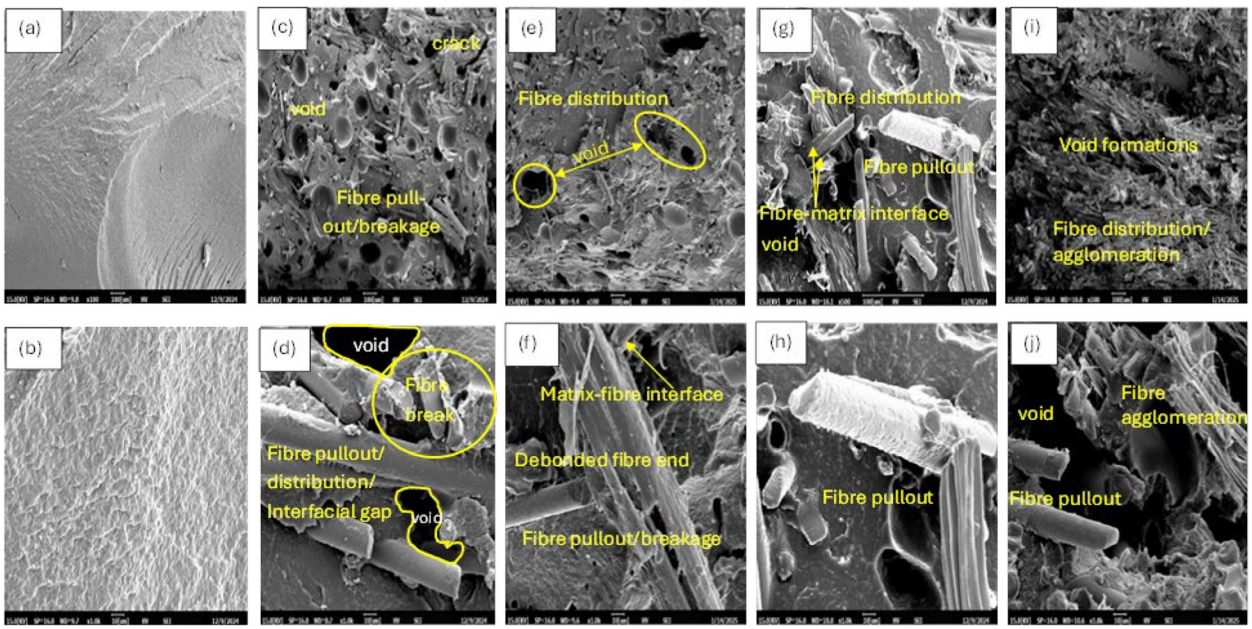

Fig. 10 SEM micrographs of hybrid TKF/GF composite: (**a**, **b**) 0%; (**c**, **d**) 20%; (**e**, **f**) 30%; (**g**, **h**) 40%; (**i**, **j**) 50%. (**b**), (**d**), (**f**), (**h**), and (**j**) are higher magnification (1000x) images of (**a**), (**c**), (**e**), (**g**) and (**j**) respectively

the hybrid fibres, with partially pulled-out fibres and visible interfacial gaps signifying moderate adhesion and the early stages of hybrid fibre (natural and synthetic) synergy [82].

Moreover, when the hybrid fibre content was increased to E3 (10 wt.% TKF and 20 wt.% GF), the observed microstructure becomes more refined, with improved dispersion of fibre, fewer voids, and stronger fibre-matrix interfacial bonding. Although, some debonding and matrix deformation zones are present. However, the minimal fibre breakage or pullout indicates an enhanced load transfer with better mechanical interlocking. This is largely attributed to the surface treatment done on the TKF to improve hydrophobicity and compatibility [83].

Similarly, the enhanced dispersion and balanced hybrid fibre ratio, helps to promote a synergistic toughening effect that is consistent with hybrid reinforcement theory [83, 84]. The E4 composite (15 wt.% TKF and 25 wt.% GF) shows similar favourable features, reinforcing this optimal interaction zone.

At the highest hybrid fibre content, E5 (20 wt.% TKF and 30 wt.% GF), the micrographs reveal signs of fibre agglomeration, voids, and fibre pullout, particularly conspicuous at higher magnifications (Fig. 10i and j). These features suggest poor dispersion of fibres having a compromised matrix continuity because of the overcrowding which hinders effective wetting. This is a common scenario associated with composites exceeding critical fibre volume [85]. The morphological evidence across all compositions indicates a varied failure mechanism involving fibre pullout, interfacial debonding, matrix plastic deformation, and fibre breakage. Notably, hybrid contents of 30-40wt.% appear to have a moderately best balance between interfacial strength and energy absorption which is critical for optimal mechanical performance. The complex patterns of stress distribution suggest that future enhancements in composite behavior could be achieved through careful selection, treatment and arrangement of fibres to adequately control interfacial properties tailored to specific application needs.

In addition, the incorporation of varying nanoclay loadings (1wt.% to 5wt.%) showed a distinct microstructural characteristic that critically influences the mechanical performance of hybrid biocomposites as shown in Fig. 11. At low nanoclay content (1wt.%), poor matrix-fibre adhesion, minimal nanoclay interaction, and low surface roughness were observed, reflecting weak reinforcement due to insufficient surface area for effective load transfer [86]. Conversely, moderate nanoclay loading (3wt.%) exhibited improved filler dispersion, tighter fibre—matrix bonding, and enhanced interfacial adhesion. These features align with an optimal balance between dispersion and mechanical enhancement [87, 88]. Ultimately, at higher clay loading (5 wt.%), significant agglomeration, re-agglomerated clay domains, and stress concentrators were observed from the micrographs, affirming that the use of excess filler beyond the percolation threshold disrupts dispersion and hampers structural performance [89].

These morphological observations clearly indicate that a 3wt.% nanoclay loading (E3-2) offers the most favorable microstructure, characterised by uniform dispersion, strong interfacial bonding, and reduced void formation. In contrast, the 1wt.% loading lacks adequate reinforcement capability, while the 5wt.% loading promotes nanoclay clustering and poor stress transfer, as consistently noted in previous studies [86, 88]. Such insights are essential for optimising nanofiller content to achieve desired structural integrity and functional performance in hybrid biocomposite applications.

Characterisation of nanoclay powder

The results of the nanoclay characterisation by the thermogravimetric analysis (TGA), FTIR spectroscopy analysis and SEM/EDX spectrum are presented in Fig. 12a, b, c and d respectively.

The thermogravimetric analysis (TGA) and derivative thermogravimetry (DTG) curves signifies that the nanoclay exhibits a multi-stage decomposition process and good thermal stability across a temperature range of 30 °C to 600 °C. The material remains stable up to around 200 °C, with minimal weight loss due to the evaporation of surface moisture. A significant weight loss occurs between 200 °C and 500 °C, attributed to the decomposition of organic modifiers like surfactants or quaternary ammonium salts, with a DTG peak at 330–350 °C marking the highest degradation rate. Beyond 500 °C, the weight stabilizes, reflecting the presence of thermally stable inorganic silicate structures. These findings align with those reported for organically modified montmorillonite clays and are crucial for evaluating the structural integrity of nanoclay and suitability for high temperature applications.

The FTIR spectroscopy analysis affirms the hybrid organic–inorganic nature of the supplied nanoclay, revealing a combination of structural clay features and organic modifications. A strong absorption band at 3628.90 cm^{-1} indicates O–H stretching from hydroxyl groups within silicate layers, characteristic of smectite-type clays like montmorillonite, reflecting a preserved layered structure. Peaks at 2919.90 cm^{-1} and 2849.98 cm^{-1} correspond to aliphatic C–H stretching, confirming the presence of quaternary ammonium salts or surfactants from organo-modification. Additional bands, including 1617.19 cm^{-1} (H–O–H bending), 1466.99 cm^{-1} (CH_2 scissoring), 988.95 cm^{-1} (Si–O stretching), 796.25 cm^{-1}

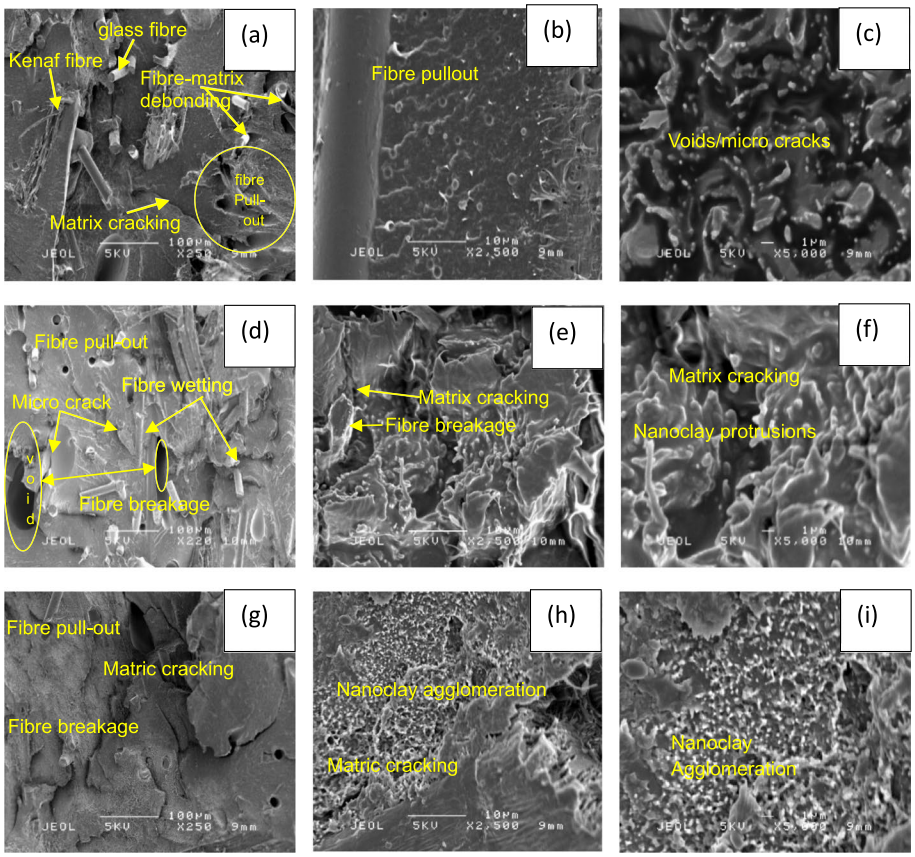

Fig. 11 SEM images of hybrid composite E3 series (E3-1, E3-2, E3-3) with different nanoclay content: (**a**-**c**) 1%, (**d**-**f**) 3%, (**g**-**i**) 5%; (**b**, **e**, **h**), and (**c**, **f**, **i**) are higher magnifications (2500 × and 5000x) images of (**a**), (**d**) and (**g**) respectively. The SEM analysis reveals that optimal hybrid fibre content (30–40 wt.%) combined with precise 3 wt.% nanoclay loading achieves exceptional microstructural uniformity, interfacial integrity, and effective stress transfer, crucially enhancing mechanical performance. Exceeding these limits promotes agglomeration, fibre overcrowding, and compromised dispersion, thereby highlighting the critical importance of tailored reinforcement strategies for advanced biocomposite applications

(Si–O–Si bending), and 722.31 cm^{-1} (CH_2 rocking), further support the coexistence of silicate frameworks and organic moieties, validating the material's structural integrity and functionalization for advanced applications.

The SEM/EDX analysis showed that the synthesized nanoclay exhibits a heterogeneous, porous morphology composed of aggregated, irregularly shaped particles, suggesting a high surface area beneficial for adsorption and catalytic applications. Elemental analysis through EDX identifies key constituents such as carbon (C), oxygen (O), iron (Fe), aluminum (Al), magnesium (Mg), chlorine (Cl), and traces of gold (Au), with gold attributed to the sputter coating used during imaging. The presence of Fe and O suggests iron oxide formation, while Al and Mg point to clay-based minerals like montmorillonite or aluminosilicates. Normalised elemental composition data show high proportions of carbon and oxygen (29.16–43.37% and 33.86–37.64%, respectively), indicating organic modification or residual carbonaceous content. Significant silicon (15.17–25.24%) and aluminum levels further confirm a silicate-based matrix, while minor amounts of Mg and Fe suggest structural substitution or functional enhancement. Trace chlorine likely originates from precursor salts used in synthesis. Together, these findings confirm a multifunctional nanoclay structure with potential applications in environmental remediation, catalysis, and nanocomposite formulation.

The comprehensive thermal, spectroscopic, and morphological analyses confirm the successful synthesis of a structurally robust and multifunctional nanoclay composite with broad application potential. Its thermal stability and distinct decomposition stages validate its suitability for high temperature uses, such as in polymer nanocomposites and flame-retardant systems. The FTIR results reveal the integration of organic functional groups within a preserved silicate framework, enhancing compatibility with hydrophobic environments and supporting applications in drug delivery and wastewater treatment. Meanwhile, SEM/EDX analysis highlights a

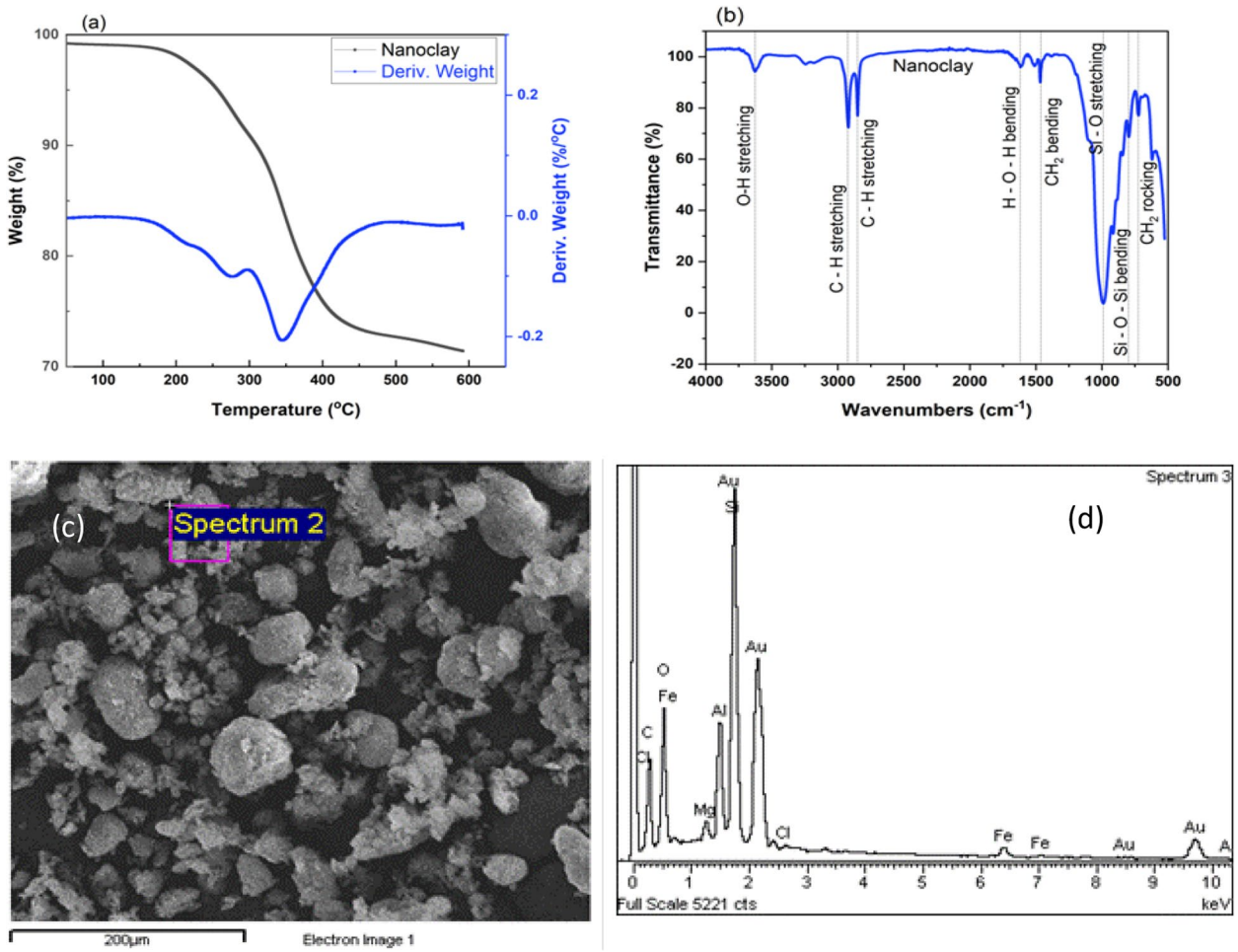

Fig. 12 Nanoclay characteristic properties (**a**) TGA-DTG curves, (**b**) FTIR peaks, (**c**) SEM micrograph, (**d**) EDX spectrum

porous morphology and a hybrid elemental composition, indicating strong potential for pollutant adsorption, catalysis, and nanocomposite reinforcement. Altogether, the balanced organic/inorganic nature of the nanoclay corroborate its versatility in diverse environmental and industrial contexts. Integrated TGA, FTIR, and SEM/EDX analyses collectively affirm the multifunctional and thermally robust nature of the synthesized nanoclay, exhibiting a distinct organic–inorganic hybrid configuration ideal for high-temperature polymer composites and advanced environmental remediation. Its hierarchical porosity and surface chemistry provide strategic interfacial interactions, highlighting its broad applicability in adsorption, catalysis, and nanostructured composite enhancement.

In summary, the enhanced interfacial adhesion observed at 3 wt.% nanoclay loading is attributed to the optimal dispersion of exfoliated silicate layers within the polyamide matrix, which facilitates effective stress transfer and interfacial interactions between the matrix and reinforcing fibres. At this concentration, the nanoclay platelets are well-dispersed and aligned, creating a tortuous path that reduces polymer chain mobility, suppresses microvoid formation, and enhances the mechanical interlocking with both treated kenaf fibre (TKF) and glass fibre (GF). Furthermore, FTIR analysis indicates increased hydrogen bonding between the amide (C=O and N–H) groups of PA6 and the hydroxyl (–OH) and silanol (Si–OH) groups present in both the treated natural fibres and the organo-modified nanoclay. This chemical affinity promotes better fibre wetting and tighter fibre–matrix interfaces. SEM images of the 3 wt.% nanoclay-loaded composite (E3-2) further confirm improved morphology, with reduced fibre pullout, minimal voids, and a continuous matrix phase, supporting the conclusion that this loading level achieves a synergistic balance between dispersion, interfacial bonding, and reinforcement. In contrast, higher nanoclay contents (e.g., 5 wt.%) lead to particle agglomeration, poor wetting, and stress

concentration sites, which diminish interfacial integrity and overall composite performance.

Conclusions

Polyamide based composites that combine hybrid fibres (TKF/GF) and nanoclay (each performing a role specific) offers a synergistic means of engineering the material's mechanical, thermal, and structural characteristics to advantage. Hybrid fibres provide stiffness and mechanical reinforcement, while nanoclay modifies moisture resistance, interfacial bonding, and thermal behavior. The strength, toughness, water absorption, and microstructural integrity of the finished composites, are among the performance criteria that are impacted by these interrelated elements as highlighted below.

Hybrid Fibre (TKF/GF) Effects:

➢ Hybrid fibre addition (20 to 50 wt.%) significantly improves flexural strength (31% approx., from 68.4 to 89.5 MPa) and flexural modulus (up to 7 GPa) due to improved interfacial bonding and fibrous reinforcement.
➢ Peak tensile strength occurs at 30 wt.% hybrid fibre loading (55 MPa), with a consistent tensile modulus (8 GPa approx.) across the 20–50 wt.% hybrid fibre loadings.
➢ Impact toughness decreases notably (from 35.3 to 18.2 kJ/m^2) with increased fibre content, reflecting rigidity and reduced energy absorption capacity.
➢ Water absorption sharply increases by over 130% with higher fibre content due to cellulose hydrophilicity.
➢ Thermal stability is enhanced, raising degradation onset temperature (from 254 °C to 301 °C) and char yield (from 17.7% to 30.3%).
➢ FTIR confirms enhanced fibre-matrix hydrogen bonding; SEM shows improved fibre wetting and optimized stress distribution between 30–40 wt.% fibres.

Nanoclay Effects:

➢ Optimal nanoclay loading (1–3 wt.%) significantly improves interfacial quality, reduces water absorption (15–30%), and enhances thermal stability by delaying degradation onset (10 to 40 °C increase) and increasing char residue (up to 37%).
➢ Peak flexural strength (95 MPa) is observed at 1 wt.% nanoclay, decreasing with higher loading due to agglomeration and porosity.
➢ Tensile strength progressively decreases with nanoclay addition (up to 45% reduction at 3 wt.%), whereas tensile modulus improves by up to 18% at high fibre (50 wt.%) and low clay loadings.
➢ Nanoclay positively impacts toughness (35.3 kJ/m^2 at E3-2 blend), enhancing crack deflection and adhesion.
➢ FTIR confirms improved polymer–clay intercalation; SEM highlights refined morphology and structural integrity due to effective nanoclay dispersion.

Recommended Formulation:

➢ Optimal performance achieved with 30–40 wt.% hybrid fibre (E3 and E4) to balance mechanical strength, interfacial adhesion, and water resistance without excessive stiffness.
➢ Ideal nanoclay content is 3 wt.%, effectively maximising thermal stability, reducing voids, improving water resistance, and avoiding agglomeration.
➢ Final recommended formulations: E3-2 and E4-2 (30–40 wt.% hybrid fibres with 3 wt.% nanoclay) suitable for advanced structural, environmental, and industrial applications.

Abbreviations

CF	Carbon fibre (CF)
LKTN)	Lembaga kenaf dan Tembakau Negara
TKF	Treated kenaf fibre
GF	Glass fibre
PA6	Nylon 6 / Polyamide 6
NC	Nanoclay
PLA	Polylactic acid
ISO	International standard
ASTM	American Standard Testing and Materials
TGA	Thermo-gravimetric analysis
FTIR	Fourier transform infrared spectroscopy analysis
SEM	Scanning electron microscopy
INTROP	Institute of Tropical Forestry and Forest Product, and
IBS	Institut Biosains
PWI	Permanent Way Institution
NaOH	Sodium hydroxide
CURT	Standards of China Urban Rail Transit
Mohurd	Ministry of Housing and Urban–Rural Development of the Peoples's Republic of China
FFU	Fibre foamed Urethane

Acknowledgements
The authors would like to thank Universiti Putra Malaysia for the financial support through the Special Graduate Research Allowance (SGRA) scholarship, Universiti Putra Malaysia Grant scheme GPB HiCOE grant VOT 521007.

Clinical trial number
Not applicable.

Institutional review board statement
Ethical review was waived due to not involving humans.

Authors' contributions
A.M.M—Conducting experiment and writing main manuscript F.N.A—Analysis and reviewed data. K.A—Editing, reviewed and owned the grant for this project S.A.R- Writing and editing manuscript.

Funding
This paper was funded by HiCOE grant (521007).

Data availability
No datasets were generated or analysed during the current study.

Declarations

Ethics approval and consent to participate
Patient consent was waived due to not involving humans.

Competing interests
The authors declare no competing interests.

Received: 10 June 2025 Accepted: 21 August 2025
Published online: 15 October 2025

References

1. D.E. Abulyazied, A. Ene, An investigative study on the progress of nanoclay-reinforced polymers: preparation, properties, and applications: a review. Polymers **13**(24), 4401 (2021). https://doi.org/10.3390/polym13244401
2. J. Parente, P.N.B. Reis, M. Neto, A.M. Amaro, Mechanical properties of sandwich composites reinforced by nanoclays: an overview. Appl. Sci. **10**, 2637 (2020). https://doi.org/10.3390/app10072637
3. M. Asensio, M. Herrero, K. Núñez, J.C. Merino, J.M. Pastor, The influence of sepiolite orientation and concentration, on the morphological, thermal and mechanical properties of bio-polyamide 4.10 nanocomposites. Polym. Eng. Sci. **60**, 1035 (2020). https://doi.org/10.1002/pen.25359
4. B. Mylsamy, S.K.M. Shanmugam, K. Aruchamy, S. Palanisamy, R. Nagarajan, N. Ayrilmis, A review on natural fiber composites: polymer matrices, fiber surface treatments, fabrication methods, properties, and applications. Polym. Eng. Sci. **64**(6), 2345–2373 (2024)
5. G. Haddou, J. Dandurand, E. Dantras, H. Maiduc, H. Thai, N.V. Giang, T.H. Trung, P. Ponteins, C. Lacabanne, Mechanical properties of continuous bamboo fiber-reinforced biobased polyamide 11 composites. J. Appl. Polym. Sci. (2019). https://doi.org/10.1002/app.47623
6. S. Armioun, S. Panthapulakkal, J. Scheel, J. Tjong, M. Sain, Sustainable and lightweight biopolyamide hybrid composites for greener auto parts. Can. J. Chem. Eng. **94**, 2052 (2016). https://doi.org/10.1002/cjce.22609
7. S. Simões, High-performance advanced composites in multifunctional material design: state of the art, challenges, and future directions. Materials **17**(23), 5997 (2024). https://doi.org/10.3390/ma17235997
8. T.H. Mahdi, M.E. Islam, M.V. Hosur, S. Jeelani, Low-velocity impact performance of carbon fiber-reinforced plastics modified with carbon nanotube, nanoclay and hybrid nanoparticles. J. Reinf. Plast. Compos. **36**, 696 (2017). https://doi.org/10.1177/0731684417693429
9. M.S. Islam, Z.A. Talib, M. Hasan, I. Ramli, M.K.M. Haafiz, M. Jawaid, A. Islam, I.M. Inuwa, Evaluation of mechanical, morphological, and biodegradable properties of hybrid natural fiber polymer nanocomposites. Polym. Compos. **38**, 583 (2017). https://doi.org/10.1002/pc.23616
10. S.M. Ahmad, M.C. Gowrishankar, M. Shettar, A review on properties of bamboo fiber polymer composites and bamboo/glass fiber/nanoclay hybrid composites. Mater. Res. Express **12**, 012002 (2025). https://doi.org/10.1088/2053-1591/ada875
11. A. Karthik, M. Bhuvaneshwaran, M.S. Senthil Kumar, S. Palanisamy, M. Palaniappan, N. Ayrilmis, A review on surface modification of plant fibers for enhancing properties of biocomposites. ChemistrySelect **9**(21), e202400650 (2024)
12. D. Zhang, C. Gao, X. Hao, G. Jing, X. Zhang, Y. Wu, X. Li, Composite materials using recycled high-density polyethylene plastic for railway sleepers. Emerg. Mater. Res. **13**, 3 (2024). https://doi.org/10.1680/jemmr.23.00050
13. Krishnasamy, K., Palanisamy, J., & Bhuvaneshwarana, M. (2024, November). A review on natural fiber reinforced biocomposites properties and its applications. In *AIP Conference Proceedings* (Vol. 3192, No. 1, p. 020015). AIP Publishing LLC.
14. Raj, S. S., Mylsamy, B., Velayutham, T., Aruchamy, K., Palaniappan, S. K., & Siengchin, S. (2025). Coating techniques for coating fibers and polymers and their stability. In *Surface Modification and Coating of Fibers, Polymers, and Composites* (pp. 313–329). Elsevier.
15. Y.F. Hu, J. Zhang, B. Wang, X.N. Zhang, Impregnation behavior of polyamide 6 in carbon fibers and the properties of their composites. Mater. Sci. Forum **898**, 2134 (2017). https://doi.org/10.4028/www.scientific.net/MSF.898.2134
16. H. Liu, H. Cui, W. Wen, X. Su, H. Kang, C. Engler-Pinto, The effect of voids on the quasi-static tensile properties of carbon fiber/polymer-laminated composites. J. Compos. Mater. **52**, 1997 (2018). https://doi.org/10.1177/0021998317737827
17. C. Wilson, E. Currens, and J. Rakow, Void content in out-of-autoclave manufacturing processes, Cambridge.Org. Microscopy and Microanalysis, •cambridge. Org **22**, 19 (2016). https://doi.org/10.1017/S143192761601000X
18. M. Fasihi and M. Abolghasemi, Oxygen barrier and mechanical properties of masterbatch-based PA6/nanoclay composite films, Wiley Online Library Journal of Applied Polymer Science, 2012•Wiley Online Library **125**, 2 (2012). https://doi.org/10.1002/app.35467
19. S. Roy, K. Narasimhan, Characterization and modelling of hygrothermal effects in thermoplastic nanocomposites. Polym. Polym. Compos. **19**, 527 (2011). https://doi.org/10.1177/096739111101900702
20. P. Santamaría and I. González, Mechanical and barrier properties of ternary nanocomposite films based on polycarbonate/amorphous polyamide blends modified with a nanoclay, Wiley Online LibraryP Santamaría, I González, JI EguiazábalPolymers for Advanced Technologies, 2015•Wiley Online Library **26**, 665 (2015). https://doi.org/10.1002/pat.3502
21. C. Kaynak, O. Polat, Influences of nanoclays on the flame retardancy of fiber-filled and unfilled polyamide-6 with and without aluminum diethylphosphinate. J. Fire Sci. **33**, 87 (2015). https://doi.org/10.1177/0734904114555961
22. A.M. Mukaddas, F.N.A. Abdul Aziz, K. Abdan, A.R. Shafi, Fabrication and characterisation of Kenaf fibre reinforced polyamide biocomposites for railway sleeper applications. Pertanika J. Sci. Technol. **32**(S5), 133 (2024). https://doi.org/10.47836/pjst.32.S5.07
23. E. Agnantopoulou, V. Tserki, S. Marras, J. Philippou, C. Panayiotou, Development of biodegradable composites based on wood waste flour and thermoplastic starch. J. Appl. Polym. Sci. **126**(S1), E273 (2012). https://doi.org/10.1002/APP.35420
24. C.H. Tay, N. Mazlan, M.T.H. Sultan, K. Abdan, C.H. Lee, Mechanical performance of hybrid glass/kenaf epoxy composite filled with organomodified nanoclay. J. Mater. Res. Technol. **15**, 4415 (2021). https://doi.org/10.1016/j.jmrt.2021.10.062
25. ISO 62, Plastics - Determination of water absorption., p. 15 (2008).
26. ASTM D790, Standard test methods for flexural properties of unreinforced and reinforced plastics and electrical insulating materials., vol. 08.01 (ASTM International, Code of Practice, West Conshohocken, PA, 2017). https://doi.org/10.1520/D0790-17
27. ASTM D638, Test method for tensile properties of plastics, vol. 08.01 (ASTM International, Code of Practice, West Conshohocken, PA, 2022). https://doi.org/10.1520/D0638-2
28. ASTM E1131, Standard test method for compositional analysis by thermogravimetry, vol. 14.01 (ASTM International, Code of Practice, West Conshohocken, PA, 2020). https://doi.org/10.1520/E1131-20
29. J. Son, H.-J. Kim, P.-W. Lee, Role of paper sludge particle size and extrusion temperature on performance of paper sludge–thermoplastic polymer composites. J. Appl. Polym. Sci. **82**, 2709 (2001). https://doi.org/10.1002/app.2123
30. H.-S. Yang, H.-J. Kim, H.-J. Park, B.-J. Lee, T.-S. Hwang, Water absorption behavior and mechanical properties of lignocellulosic filler–polyolefin bio-composites. Compos. Struct. **72**, 429 (2006). https://doi.org/10.1016/j.compstruct.2005.01.013
31. M.H. Esmaeili, H. Norouzi, F. Niazi, Evaluation of mechanical and performance characteristics of a new composite railway sleeper made from recycled plastics, mineral fillers and industrial wastes. Composites Part B: Engineering **254**, 110581 (2023). https://doi.org/10.1016/j.compositesb.2023.110581
32. N. Rull, R.P. Ollier, G. Francucci, E.S. Rodriguez, V.A. Alvarez, Effect of the addition of nanoclays on the water absorption and mechanical properties of glass fiber/up resin composites. J. Compos. Mater. **49**, 1629 (2015). https://doi.org/10.1177/0021998314538869

33. J. Naveen, M. Jawaid, E.S. Zainudin, M. T. Hameed. Sultan, R. Yahaya, Improved mechanical and moisture-resistant properties of woven hybrid epoxy composites by graphene nanoplatelets (GNP). Materials **12**(8), 1249 (2019). https://doi.org/10.3390/ma12081249
34. S.S. Chee, M. Jawaid, M.T.H. Sultan, O.Y. Alothman, L.C. Abdullah, Effects of nanoclay on physical and dimensional stability of bamboo/kenaf/nanoclay reinforced epoxy hybrid nanocomposites. J. Mater. Res. Technol. **9**, 5871 (2020). https://doi.org/10.1016/j.jmrt.2020.03.114
35. M. Eesaee, A. Shojaei, Effect of nanoclays on the mechanical properties and durability of novolac phenolic resin/woven glass fiber composite at various chemical environments. Compos. Part A Appl. Sci. Manuf. **63**, 149 (2014). https://doi.org/10.1016/j.compositesa.2014.04.008
36. T. J. Nosker and A. Tewatia, Development, testing, and application of recycled plastic composite sleepers, PermanentWayInstitution(PWI) FinalTechnicalJournal (2019).
37. V. Fiore, G. Di Bella, A. Valenza, The effect of alkaline treatment on mechanical properties of kenaf fibers and their epoxy composites. Composites Part B: Engineering **68**, 14 (2015). https://doi.org/10.1016/J.COMPOSITESB.2014.08.025
38. N.I.A. Razak, N.A. Ibrahim, N. Zainuddin, M. Rayung, W.Z. Saad, The influence of chemical surface modification of kenaf fiber using hydrogen peroxide on the mechanical properties of biodegradable kenaf fiber/poly(lactic acid) composites. Molecules **19**, 2957 (2014). https://doi.org/10.3390/MOLECULES19032957
39. N. Abdullah, K. Abdan, C.H. Lee, M.H. Mohd Roslim, M.N. Radzuan, A.R. shafi, Thermal properties of wood flour reinforced polyamide 6 biocomposites by twin screw extrusion. Phys. Sci. Rev. **8**, 5153 (2023). https://doi.org/10.1515/psr-2022-0082
40. ISO 12856-1, Railway applications - Polymeric composite sleepers, bearers and transoms, Part 1: Material Characteristics 43 (2022)
41. E. Dias, H. Chalse, S. Mutha, Y. Mundhe, N. Ambhore, A. Kulkarni, A. Mache, Review on synthetic/natural fibers polymer composite filled with nanoclay and their mechanical performance. Mater. Today Proc. **77**, 916 (2023). https://doi.org/10.1016/j.matpr.2022.12.059
42. B. Mylsamy, S.K. Palaniappan, S.P. Subramani, S.K. Pal, K. Aruchamy, Impact of nanoclay on mechanical and structural properties of treated *Coccinia indica* fibre reinforced epoxy composites. J. Mater. Res. Technol. **8**, 6021 (2019). https://doi.org/10.1016/j.jmrt.2019.09.076
43. R. Fidalgo-Pereira, Ó. Carvalho, S.O. Catarino, B. Henriques, O. Torres, A. Braem, J.C.M. Souza, Effect of inorganic fillers on the light transmission through traditional or flowable resin-matrix composites for restorative dentistry. Clin. Oral Invest. **27**, 5679 (2023). https://doi.org/10.1007/s00784-023-05189-7
44. H.H.K. Xu, Whisker-reinforced heat-cured dental resin composites: effects of filler level and heat-cure temperature and time. J. Dent. Res. **79**, 1392 (2000). https://doi.org/10.1177/00220345000790060701
45. M.H. Gabr, N.T. Phong, M.A. Abdelkareem, K. Okubo, K. Uzawa, I. Kimpara, T. Fujii, Mechanical, thermal, and moisture absorption properties of nanoclay reinforced nano-cellulose biocomposites. Cellulose **20**, 819 (2013). https://doi.org/10.1007/S10570-013-9876-8
46. H.S. Lee, D. Cho, S.O. Han, Effect of natural fiber surface treatments on the interfacial and mechanical properties of henequen/polypropylene biocomposites. Macromol. Res. **16**, 411 (2008). https://doi.org/10.1007/BF03218538
47. M. Šupová, G.S. Martynková, K. Barabaszová, Effect of nanofillers dispersion in polymer matrices: a review. Sci. Adv. Mater. (2011). https://doi.org/10.1166/SAM.2011.1136
48. Y. Zare, K.Y. Rhee, D. Hui, Influences of nanoparticles aggregation/agglomeration on the interfacial/interphase and tensile properties of nanocomposites. Composites Part B: Engineering **122**, 41 (2017). https://doi.org/10.1016/j.compositesb.2017.04.008
49. G.E. Rani, R. Murugeswari, S. Siengchin, N. Rajini, M.A. Kumar, Quantitative assessment of particle dispersion in polymeric composites and its effect on mechanical properties. J. Mater. Res. Technol. **19**, 1836 (2022). https://doi.org/10.1016/j.jmrt.2022.05.147
50. A. Takahashi, Y. Sato, S. Uno, P.N.R. Pereira, H. Sano, Effects of mechanical properties of adhesive resins on bond strength to dentin. Dent. Mater. **18**, 263 (2002). https://doi.org/10.1016/S0109-5641(01)00046-X
51. H. Oliver-Ortega, M.F. Llop, F.X. Espinach, Q. Tarrés, M. Ardanuy, P. Mutjé, Study of the flexural modulus of lignocellulosic fibers reinforced biobased polyamide11 green composites. Composites Part B: Engineering **152**, 126 (2018). https://doi.org/10.1016/j.compositesb.2018.07.001
52. N.A. Siddiqui, R.S.C. Woo, J.K. Kim, C.C.K. Leung, A. Munir, Mode I interlaminar fracture behavior and mechanical properties of CFRPs with nanoclay-filled epoxy matrix. Compos. Part A Appl. Sci. Manuf. **38**, 449 (2007). https://doi.org/10.1016/j.compositesa.2006.03.001
53. A. Atiqah, M.A. Maleque, M. Jawaid, M. Iqbal, Development of kenaf-glass reinforced unsaturated polyester hybrid composite for structural applications. Composites Part B: Engineering **56**, 68 (2014). https://doi.org/10.1016/j.compositesb.2013.08.019
54. M.H. Pol, G.H. Liaghat, Studies on the mechanical properties of composites reinforced with nanoparticles. Polym. Compos. **38**, 205 (2017). https://doi.org/10.1002/pc.23577
55. S.M. Ahmad, G.M. C, M. Shettar, S. Sharma, Experimental investigation of mechanical properties and morphology of bamboo-glass fiber-nanoclay reinforced epoxy hybrid composites. Cogent Engineering (2023). https://doi.org/10.1080/23311916.2023.2279209
56. P. Yu, A. Manalo, W. Ferdous, R. Abousnina, C. Salih, T. Heyer, P. Schubel, Investigation on the physical, mechanical and microstructural properties of epoxy polymer matrix with crumb rubber and short fibres for composite railway sleepers. Constr. Build. Mater. **295**, 123700 (2021)
57. Y. Wang, Z. Zhang, and X. Zhang, Characteristic of fresh and harden properties of polyvinyl alcohol fibre reinforced alkali activated composite, J Renew Mater 11, 1321 (2023). https://doi.org/10.32604/jrm.2022.023266
58. H. Serin, Ş Yıldızhan, Tensile properties and cost-property efficiency analyses of expanded polystyrene/chopped glass fiber/epoxy novel composite. J. Mech. Sci. Technol. **35**, 145 (2021). https://doi.org/10.1007/s12206-020-1213-1
59. D. Hernández-Díaz, R. Villar-Ribera, F.X. Espinach, F. Julián, V. Hernández-Abad, M. Delgado-Aguilar, Impact properties and water uptake behavior of old newspaper recycled fibers-reinforced polypropylene composites. Materials **13**, 1079 (2020). https://doi.org/10.3390/ma13051079
60. M. Ates, S. Karadag, A.A. Eker, B. Eker, Polyurethane foam materials and their industrial applications. Polym. Int. **71**, 1157 (2022). https://doi.org/10.1002/pi.6441
61. A.S. Shanour, A.A. Khalil, H.S. Riad, H.M. Bakry, Experimental and analytical investigations of innovative composite materials using GFRP and iron slag for railway sleepers. J. Eng. Res. Rep. **13**, 25 (2020). https://doi.org/10.9734/jerr/2020/v13i217098
62. L. Lyu, D. Zhang, Y. Tian, X. Zhou, Sound-absorption performance and fractal dimension feature of Kapok fibre/polycaprolactone composites. Coatings **11**, 1000 (2021). https://doi.org/10.3390/coatings11081000
63. J.O. Olusanya, T.P. Mohan, K. Kanny, Fracture toughness of hybrid natural fiber/nanoclay reinforced starch biocomposite material. Composites and Advanced Materials **32**, 1 (2023). https://doi.org/10.1177/26349833231188980
64. A. Chaurasia, R.S. Mulik, A. Parashar, Polymer-based nanocomposites for impact loading: a review. Mech. Adv. Mater. Struct. **29**, 2581 (2022). https://doi.org/10.1080/15376494.2021.1871688
65. V. Krasinskyi, L. Dulebova, I. Gajdoš, O. Krasinska, T. Jachowicz, Study of crystalline and thermal properties of nanocomposites based on polyamide-6 and modified montmorillonite. Adv. Sci. Technol. Res. J. **17**, 88 (2023). https://doi.org/10.12913/22998624/174180
66. X. Zhang and L. Loo, Synthesis and thermal oxidative degradation of a novel amorphous polyamide/nanoclay nanocomposite, ElsevierX Zhang, LS LooPolymer, 2009•Elsevier (2009).
67. M.H. Mat Yazik, M.T.H. Sultan, A.U.M. Shah, M. Jawaid, N. Mazlan, Effect of nanoclay content on the thermal, mechanical and shape memory properties of epoxy nanocomposites. Polym. Bull. **77**, 5913 (2020). https://doi.org/10.1007/s00289-019-03049-7

68. H. Naderi-Samani and M. Loghman-Estarki, Water-based polyamide imide–nanoclay coating: Preparation, characterization, thermal stability and visible transparency, Elsevier (2016).
69. B. Kord, P. Ravanfar, N. Ayrilmis, Influence of organically modified nanoclay on thermal and combustion properties of bagasse reinforced HDPE nanocomposites. J. Polym. Environ. **25**, 1198 (2017). https://doi.org/10.1007/s10924-016-0897-x
70. S. J. Dahiya, Polyamide 66/nanoclay composites: synthesis, thermal and flammability properties, Aml.laamonline.OrgS JB DahiyaAdvanced Materials Letters, 2012•aml.laamonline.Org **2012**, 381 (2012). https://doi.org/10.5185/amlett.2012.5354
71. A. Célino, S. Fréour, F. Jacquemin, and P. Casari, The hygroscopic behavior of plant fibers: A review, Front Chem **1**, (2014). https://doi.org/10.3389/FCHEM.2013.00043/FULL
72. M. Mohammed, R. Rahman, A.M. Mohammed, B.O. Betar, A.F. Osman, T. Adam, O.S. Dahham, S.C.B. Gopinath, Improving hydrophobicity and compatibility between kenaf fiber and polymer composite by surface treatment with inorganic nanoparticles. Arab. J. Chem. **15**, 104233 (2022). https://doi.org/10.1016/j.arabjc.2022.104233
73. M.T. Caccamo, G. Mavilia, L. Mavilia, D. Lombardo, S. Magazù, Self-assembly processes in hydrated Montmorillonite by FTIR investigations. Materials **13**, 1100 (2020). https://doi.org/10.3390/ma13051100
74. V. Mittal, R. Saini, and S. Sinha, Natural fiber-mediated epoxy composites–a review, Elsevier (2016).
75. D. Kherroub, M. Belbachir, S. Lamouri, L. Bouhadjar, and K. Chikh, Synthesis of polyamide-6/montmorillonite nanocomposites by direct in-situ polymerization catalysed by exchanged clay, Academia.EduDE Kherroub, M Belbachir, S Lamouri, L Bouhadjar, K ChikhOriental Journal of Chemistry, 2013•academia.Edu (2013).
76. M. Qi, L. Zheng, C. Li, Y. Xiao, J. Liu, S. Wu, B. Zhang, The yellowing mechanism of polyesteramide based on poly(ethylene terephthalate) and polyamide 6. J. Appl. Polym. Sci. (2021). https://doi.org/10.1002/app.49986
77. D.I. Kis, A. Bata, J. Takács, E. Kókai, Mechanical properties of clay-reinforced polyamide 6 nanocomposite liner materials of type IV hydrogen storage vessels. Nanomaterials **14**, 1385 (2024). https://doi.org/10.3390/nano14171385
78. Q. Wu, X. Liu, L.A. Berglund, FT-IR spectroscopic study of hydrogen bonding in PA6/clay nanocomposites. Polymer **43**, 2445 (2002). https://doi.org/10.1016/S0032-3861(01)00810-2
79. D. Shelly, V. Singhal, S. Singh, T. Nanda, R. Mehta, S.-Y. Lee, S.-J. Park, Exploring the impact of nanoclay on epoxy nanocomposites: a comprehensive review. J. Compos. Sci. **8**, 506 (2024). https://doi.org/10.3390/jcs8120506
80. R. J. Sammons, D. P. Harper, N. Labbé, J. J. Bozell, T. Elder, and T. G. Rials, Characterization of organosolv lignins using thermal and FT-IR spectroscopic analysis, Research.Fs.Usda.GovRJ Sammons, DP Harper, N Labbé, JJ Bozell, T Elder, TG RialsBioResources 8 (2): 2752–2767, 2013•research.Fs.Usda.Gov **8**, 2752 (2013).
81. A.Q.F. Ahmad, H.S. Choi, M.K. Park, A review: natural fiber composites selection in view of mechanical, light weight, and economic properties. Macromol. Mater. Eng. **300**, 10 (2015). https://doi.org/10.1002/MAME.201400089
82. M. Jawaid, S. Awad, H. Fouad, M. Asim, N. Saba, H.N. Dhakal, Improvements in the thermal behaviour of date palm/bamboo fibres reinforced epoxy hybrid composites. Compos. Struct. **277**, 114644 (2021). https://doi.org/10.1016/j.compstruct.2021.114644
83. M. Jawaid, M. Sultan, and N. Saba, *Failure Analysis in Biocomposites, Fibre-Reinforced Composites and Hybrid Composites* (Elsevier, 2019). https://doi.org/10.1016/C2016-0-04423-6
84. L. Yan, N. Chouw, K. Jayaraman, Flax fibre and its composites–a review. Composites Part B: Engineering (2014). https://doi.org/10.1016/j.compositesb.2013.08.014
85. K. Pickering, M. Efendy, and T. Le, A review of recent developments in natural fibre composites and their mechanical performance, ElsevierKL Pickering, MGA Efendy, TM LeComposites Part A: Applied Science and Manufacturing, 2016•Elsevier (2016).
86. S.S. Chee, M. Jawaid, O.Y. Alothman, H. Fouad, Effects of nanoclay on mechanical and dynamic mechanical properties of bamboo/kenaf reinforced epoxy hybrid composites. Polymers **13**(3), 395 (2021). https://doi.org/10.3390/polym13030395
87. A.H. Alias et al., Hybridization of MMT/lignocellulosic fiber reinforced polymer nanocomposites for structural applications: a review. Coatings **11**(11), 1355 (2021). https://doi.org/10.3390/coatings11111355
88. C.I. Idumah, C.M. Obele, E.O. Ezeani, Understanding interfacial dispersions in ecobenign polymer nano-biocomposites. Polym.-Plast. Technol. Eng. **60**, 233 (2021). https://doi.org/10.1080/25740881.2020.1811312
89. A.U. Kini, M. Shettar, M.C. Gowrishankar, S. Sharma, A technical review on epoxy-nanoclay nanocomposites: mechanical, hygrothermal and wear properties. Cogent Engineering (2023). https://doi.org/10.1080/23311916.2023.2257949

Publisher's Note

Terms and Conditions

Springer Nature journal content, brought to you courtesy of Springer Nature Customer Service Center GmbH (“Springer Nature”).
Springer Nature supports a reasonable amount of sharing of research papers by authors, subscribers and authorised users (“Users”), for small-scale personal, non-commercial use provided that all copyright, trade and service marks and other proprietary notices are maintained. By accessing, sharing, receiving or otherwise using the Springer Nature journal content you agree to these terms of use (“Terms”). For these purposes, Springer Nature considers academic use (by researchers and students) to be non-commercial.
These Terms are supplementary and will apply in addition to any applicable website terms and conditions, a relevant site licence or a personal subscription. These Terms will prevail over any conflict or ambiguity with regards to the relevant terms, a site licence or a personal subscription (to the extent of the conflict or ambiguity only). For Creative Commons-licensed articles, the terms of the Creative Commons license used will apply.
We collect and use personal data to provide access to the Springer Nature journal content. We may also use these personal data internally within ResearchGate and Springer Nature and as agreed share it, in an anonymised way, for purposes of tracking, analysis and reporting. We will not otherwise disclose your personal data outside the ResearchGate or the Springer Nature group of companies unless we have your permission as detailed in the Privacy Policy.
While Users may use the Springer Nature journal content for small scale, personal non-commercial use, it is important to note that Users may not:

1. use such content for the purpose of providing other users with access on a regular or large scale basis or as a means to circumvent access control;
2. use such content where to do so would be considered a criminal or statutory offence in any jurisdiction, or gives rise to civil liability, or is otherwise unlawful;
3. falsely or misleadingly imply or suggest endorsement, approval , sponsorship, or association unless explicitly agreed to by Springer Nature in writing;
4. use bots or other automated methods to access the content or redirect messages
5. override any security feature or exclusionary protocol; or
6. share the content in order to create substitute for Springer Nature products or services or a systematic database of Springer Nature journal content.

In line with the restriction against commercial use, Springer Nature does not permit the creation of a product or service that creates revenue, royalties, rent or income from our content or its inclusion as part of a paid for service or for other commercial gain. Springer Nature journal content cannot be used for inter-library loans and librarians may not upload Springer Nature journal content on a large scale into their, or any other, institutional repository.
These terms of use are reviewed regularly and may be amended at any time. Springer Nature is not obligated to publish any information or content on this website and may remove it or features or functionality at our sole discretion, at any time with or without notice. Springer Nature may revoke this licence to you at any time and remove access to any copies of the Springer Nature journal content which have been saved.
To the fullest extent permitted by law, Springer Nature makes no warranties, representations or guarantees to Users, either express or implied with respect to the Springer nature journal content and all parties disclaim and waive any implied warranties or warranties imposed by law, including merchantability or fitness for any particular purpose.
Please note that these rights do not automatically extend to content, data or other material published by Springer Nature that may be licensed from third parties.
If you would like to use or distribute our Springer Nature journal content to a wider audience or on a regular basis or in any other manner not expressly permitted by these Terms, please contact Springer Nature at

onlineservice@springernature.com